Atmos. Meas. Tech. Discuss., 7, 1691–1747, 2014
www.atmos-meas-tech-discuss.net/7/1691/2014/
doi:10.5194/amtd-7-1691-2014

Atmospheric Measurement Techniques Discussions
Open Access

Retrieval of carbon dioxide vertical profiles from solar occultation observations and associated error budgets for ACE-FTS and CASS-FTS

C. E. Sioris[1], C. D. Boone[2], R. Nassar[3], K. J. Sutton[4], I. E. Gordon[5], K. A. Walker[6], and P. F. Bernath[7]

[1]Department of Earth and Space Science and Engineering, York University, Toronto, ON, Canada
[2]Department of Chemistry, University of Waterloo, Waterloo, ON, Canada
[3]Climate Research Division, Environment Canada, Toronto, ON, Canada
[4]Department of Physics and Astronomy, University of Waterloo, Waterloo, ON, Canada
[5]Atomic and Molecular Physics Division, Harvard-Smithsonian Center for Astrophysics, Cambridge, MA, USA
[6]Department of Physics, University of Toronto, Toronto, ON, Canada
[7]Department of Chemistry and Biochemistry, Old Dominion University, Norfolk, VA, USA

Received: 5 February 2014 – Accepted: 10 February 2014 – Published: 18 February 2014

Correspondence to: C. E. Sioris (csioris@cfa.harvard.edu)

Published by Copernicus Publications on behalf of the European Geosciences Union.

AMTD
7, 1691–1747, 2014

Abstract

An algorithm is developed to retrieve the vertical profile of carbon dioxide in the 5 to 25 km altitude range using mid-infrared solar occultation spectra from the main instrument of the ACE (Atmospheric Chemistry Experiment) mission, namely the Fourier Transform Spectrometer (FTS). The main challenge is to find an atmospheric phenomenon which can be used for accurate tangent height determination in the lower atmosphere, where the tangent heights (THs) calculated from geometric and timing information is not of sufficient accuracy. Error budgets for the retrieval of CO_2 from ACE-FTS and the FTS on a potential follow-on mission named CASS (Chemical and Aerosol Sounding Satellite) are calculated and contrasted. Retrieved THs are typically within 60 m of those retrieved using the ACE version 3.x software after revisiting the temperature dependence of the N_2 CIA (Collision-Induced Absorption) laboratory measurements and accounting for sulfate aerosol extinction. After correcting for the known residual high bias of ACE version 3.x THs expected from CO_2 spectroscopic/isotopic inconsistencies, the remaining bias for tangent heights determined with the N_2 CIA is −20 m. CO_2 in the 5–13 km range in the 2009–2011 time frame is validated against aircraft measurements from CARIBIC, CONTRAIL and HIPPO, yielding typical biases of −1.7 ppm in the 5–13 km range. The standard error of these biases in this vertical range is 0.4 ppm. The multi-year ACE-FTS dataset is valuable in determining the seasonal variation of the latitudinal gradient which arises from the strong seasonal cycle in the Northern Hemisphere troposphere. The annual growth of CO_2 in this time frame is determined to be 2.5 ± 0.7 ppm yr^{-1}, in agreement with the currently accepted global growth rate based on ground-based measurements.

AMTD
7, 1691–1747, 2014

1 Introduction

Besides water vapour, carbon dioxide is the most important greenhouse gas. Its concentration in the atmosphere has been rising at an increasing rate for decades (Hofmann et al., 2009), with a rate of 1.66–2.44 ppm yr^{-1} in the 2009–2012 period for the background global mean (http://www.esrl.noaa.gov/gmd/ccgg/trends/global.html). There is growing global concern about the consequential climate change with its broad spectrum of impacts on life across the planet. Efforts to curb the atmospheric growth of this greenhouse gas are difficult because of its long atmospheric lifetime and our dependence on fossil fuels. Nonetheless, a thorough scientific understanding of the budget of CO_2, a gas innate to life on this planet, is needed. To address this need, a wide range of measurements (concentrations, fluxes, isotopes) and modeling tools are being developed. Satellite-based remote sensing provides a global view, although the vertical distribution of CO_2, which is a very important piece of observational information, is sparse or lacking. CO_2 (volume mixing ratio) VMR profiles in the mesosphere (above $\sim$ 70 km) and lower thermosphere have been retrieved globally from observations by the Atmospheric Chemistry Experiment – Fourier Transform Spectrometer (ACE-FTS) where tangent heights are determined from geometric information (Beagley et al., 2009; Emmert et al., 2011). Because this approach is generally not of sufficient quality in the lower stratosphere and troposphere to measure CO_2, limb-viewing thermal infrared sounders such as the Michelson Interferometer for Passive Atmospheric Sounding (Fischer et al., 2008) and High Resolution Dynamics Limb Sounder (HIRDLS, Gille et al., 2008) use CO_2 simply for tangent height and temperature determination and sacrifice the opportunity to measure the VMR profile.

This was also the case with ACE-FTS until recently (Foucher et al., 2009). ACE-FTS is onboard SCISAT and was launched in August 2003. The measurements are performed at sunrise and sunset using the solar occultation technique, which, by the design of the experiment, provides the advantages of high signal-to-noise ratio, self-calibration and well-known atmospheric pathlengths, ultimately translating to retrieval

AMTD
7, 1691–1747, 2014

accuracy. The spectral range is 750–4400 cm^{-1} (2.3–13.3 µm) and the spectral resolution is 0.02 cm^{-1}. The orbital inclination of 74° results in better coverage of high latitudes, but the tropics are probed in four months of the year, covering the four seasons. More than a decade after launch, ACE-FTS continues to have a signal to noise ratio (SNR) of ∼ 400 in the 4 µm region, as determined by analysis of spectra at the highest tangent heights (130–150 km). In the other relevant spectral region (7 µm), the SNR is 300 to 400 (e.g. Châteauneuf et al., 2005).

In this work, we improve the retrieval of vertical profiles particularly via major improvements to the tangent height determination. We also perform comprehensive error budgets for ACE-FTS and the FTS on the proposed CASS (Chemical and Aerosol Sounding Satellite) mission (Melo et al., 2013).

2 Method

Retrieval of CO_2 and tangent height in this work builds on previous algorithm development by Boone et al. (2005), Foucher (2009), Foucher et al. (2009, 2011), and Rinsland et al. (2010). As discussed by Boone et al. (2005), below ∼ 43 km, tangent heights (THs) cannot be accurately determined from the geometric information (satellite position and instrument viewing angle) and thus atmospheric observables are exploited for this purpose. The ACE version 2.2 (v2.2) and v3.x (v3.0 and v3.5) retrieval algorithms (Boone et al., 2005, 2013) use CO_2 absorption lines, but the retrieval problem becomes circular if one wants to retrieve CO_2 VMR using THs determined with absorption by this molecule. Other atmospheric molecules which have thermal infrared absorption and could possibly be used for tangent height determination include O_2 and N_2 because their VMRs are well known, and constant through the troposphere and stratosphere. The O_2 magnetic dipole and electric quadrupole vibrational fundamental bands, the N_2 electric quadrupole vibrational fundamental and the O_2 and N_2 collision-induced absorption (CIA) vibrational fundamentals are essentially the five options excluding CO_2. In theory, the O_2 and N_2 lines would be preferable to N_2 CIA because there would be

AMTD
7, 1691–1747, 2014

no bias due to non-opaque clouds and the upper altitude would be much higher (e.g. 48 km for N_2 quadrupole vs. ~ 25 km for N_2 CIA). If we could demonstrate that the VMR of N_2 could be retrieved accurately using its quadrupole lines, then one would expect that tangent heights retrieved from these lines would also be accurate. However, even though non-local thermodynamic equilibrium in N_2 absorption measurements below 35 km is expected to be a small to negligible effect (e.g. Goldman et al., 2007), the retrieval of N_2 from the quadrupole line does not have the necessary precision and suffers from a low bias at the lowest altitudes. We were able to improve the N_2 VMR retrieval from the quadrupole lines compared to those retrieved using the ACE-FTS v3.x algorithm by adding lines with higher rotational quantum numbers, but ultimately the retrieval remained significantly biased relative to the expected 78 % VMR of N_2 (see also Goldman et al., 2007); the N_2 line parameters are not satisfactory. Regarding O_2, we found that the retrieval could not be extended below 15 km because of saturating H_2O lines and therefore the O_2 magnetic dipole lines did not meet our goal of retrieving into the troposphere globally. This same interference would affect a TH retrieval using the O_2 CIA.

ACE-FTS has a circular field of view of 1.25 mrad with a diameter of 3 to 4 km at the tangent point. Vertical sampling distance is dependent on the tangent height and the angle between the satellite velocity vector and the line-of-sight, namely the beta angle. In the troposphere and lowermost stratosphere, the vertical sampling is typically ~ 1 km. ACE-FTS profiles are not perfectly vertical since the satellite motion results in a difference in the satellite position for each tangent point. For low beta angles, the horizontal displacement of the tangent point during a limb scan is negligible, but for high beta angles, it can reach 400 km over the 5–25 km altitude range.

The modified global fitting method is used (Boone et al., 2005), and tangent heights are retrieved simultaneously with CO_2 VMRs. The ACE-FTS v3.x retrieval software was adapted for this application. One of the main modifications was to fit the scale and slope parameters (Boone et al., 2005) for the microwindows targeting CO_2 but not for the microwindows targeting N_2 CIA.

AMTD
7, 1691–1747, 2014

Considering all of the microwindows listed in Tables 1–2 below, the significant interferers are $^{18}O^{12}C^{16}O$, $^{17}O^{12}C^{16}O$, $^{12}CH_4$, $^{13}CH_4$, $^{14}N^{14}N^{16}O$, $^{15}N^{14}N^{16}O$, $^{14}N^{14}N^{18}O$, $H_2^{17}O$, and HOD. For these species, the vertical profiles of VMR, normalized by their standard natural isotopic abundance, are assumed to be equal to the VMR of their respective primary isotopologue, recovered using version 3.x of the ACE-FTS retrieval software (Boone et al., 2013). The sensitivity to this assumption is checked in the error budget (Sect. 2.2).

The Lafferty et al. (1996) N_2 CIA lab measurements are considered to be the best available for temperatures below 300 K according to Richard et al. (2012). The stated uncertainties in the Lafferty et al. absorption coefficients are in the 0.71 % to 0.9 % range if the uncertainty in the background spectra is added in quadrature to the uncertainty from the absorption spectra. Menoux et al. (1993) state the uncertainty in their measurements above 2470 cm^{-1} rises from 5 % (near the band center) to 10 %. The empirical model proposed by Lafferty et al. (1996) is:

$$B(\nu,T) = B_0(\nu)\exp[\beta_0(\nu)(1/T_0 - 1/T)] \quad (1)$$

where ν is the wavenumber (cm^{-1}), T is the temperature (K), and T_0 is the reference temperature of 296 K. B_0 and β_0 are the model parameters which are independent and dependent on temperature, respectively. B_0 represents the absorption coefficient of N_2-N_2 at 296 K while β_0 represents its temperature dependence at this reference temperature. In reality, β_0 is determined using the spectra at five different temperatures in the range 228.2–272.1 K available in the High resolution transmission (HITRAN) 2012 database (Rothman et al., 2013), and the empirical law in Eq. (1). We determine the best $\beta_0(\nu)$ on the 0.25 cm^{-1} grid of the Lafferty et al. (1996) measurements by absolute difference minimization of Eq. (1) at each wavenumber increment independently. This involves interpolating $B_0(\nu)$ from Table 1 of Lafferty et al. (1996) to the 0.25 cm^{-1} grid. We then average the best $\beta_0(\nu)$ in 5 cm^{-1} bins in the 2130 to 2600 cm^{-1} range to reduce noise (Fig. 1). In order to test the precision of the empirical model, we obtain five spectral simulations of B_0 by dividing the five observed $B(T)$ spectra by the exponential

AMTD
7, 1691–1747, 2014

function on the right hand side of Eq. (1) inserting the appropriate T in each case as well as the best-fit β_0 spectrum (obtained using the spectra at all five temperatures). The standard deviation of the five $B_0(\nu)$ spectra (Fig. 2) is a measure of the consistency of the observed spectra and also reflects any inaccuracy in the empirical model. The relative uncertainties in B_0 based on the standard deviation is similar to the quoted uncertainty (see above), except that at the low and high frequency ends of the band, the relative uncertainty clearly exceeds 1 %, similar to the frequency-dependence of the uncertainty found by Menoux et al. (1993).

We also determined the temperature dependence from the dataset provided by Menoux et al. (1993) but it did not improve the retrieved tangent heights when applied for wavenumbers $\leq 2600\,\mathrm{cm}^{-1}$ (the upper limit of Lafferty's published measurements). We use the Menoux et al. measurements to determine the density-normalized N_2-N_2 CIA coefficients at 296 K and their temperature dependence (following Lafferty et al., 1996) in order to extend the N_2 CIA empirical model out to $2640\,\mathrm{cm}^{-1}$. For this work, we have applied a uniform increase to the B_0 spectrum of Lafferty et al. (1996) of 0.9 % and additionally by 0.1 % and 0.2 % at 2500 and 2505–2510 cm^{-1}, respectively. These increases are within the uncertainties shown in Fig. 2.

Lafferty et al. (1996) published the following fit to the temperature dependence of the relative N_2 collision efficiency with O_2 vs. collision with itself (N_2) of:

$$E^{N_2}_{O_2/N_2}(T) = 1.294 - 0.4545T/T_0 \quad (2)$$

Absorption due to N_2-H_2O collisional complexes (Baranov et al., 2012) is neglected. This is a safe assumption for the upper troposphere and lower stratosphere where water vapour is typically < 0.1 % of air by volume. Using Eqs. (1)–(2) and the temperature dependence shown in Fig. 1, as well as 0.7808 and 0.2095 for the VMRs of N_2 and O_2, we obtained a slightly modified version of Eq. (8) of Lafferty et al. (1996).

AMTD
7, 1691–1747, 2014

2.1 Retrieval setup and microwindows

The HITRAN 2012 database (Rothman et al., 2013) is used in this work whereas ACE v3.x relies on HITRAN 2004 (with some updates) (Boone et al., 2013).

Microwindows have one of four targets:

1. cloud
2. TH (via N_2 CIA)
3. CO_2
4. aerosol

Cloud detection is carried out as a pre-processing step before the CO_2 profile retrieval. Following Foucher (2009), observed spectral transmittance profiles at 970 and 2505.5 cm^{-1} are used for cloud detection. Microwindow widths are narrow so that each cloud microwindow consists of a single point (to speed up processing). No spectral averaging is necessary. Only tangent heights below 20.0 km are searched for clouds. At 970 cm^{-1}, when the transmittance falls below 0.8 or when the change in transmittance between adjacent tangent heights exceeds 0.0689, there is considered to be a cloud. Similarly at 2505.5 cm^{-1}, if the change in transmittance between adjacent tangent heights exceeds an empirically-determined value of 0.076, a cloud is assumed to be present. The CO_2 retrieval is not applied to cloudy occultations. These empirical settings are very stringent for the purpose of reducing cloud-related error in the determination of THs and some false positives may be present (i.e. occultation is flagged as cloudy when it is not). Out of 16 676 available occultations in the 2009–2011 time period, 77 % are deemed to be cloudy and not processed and an additional 15 % are cloudy only at 2505.5 cm^{-1} and are processed (see below). The remaining 8 % constitute the cloud-free dataset.

To retrieve tangent heights via the N_2 CIA, we use the 12 microwindows in Table 1. For the microwindows at 2505, 2492.1, and 2462 cm^{-1}, the central frequencies and

AMTD
7, 1691–1747, 2014

widths were specified in Foucher et al. (2009). The centre frequencies for the first and third microwindows were obtained via private communication with Foucher. Foucher et al. (2011) mentioned the use of a microwindow at 2430 cm^{-1}. We have optimized the microwindow centre and width in terms of interfering absorption. We found that the tangent heights retrieved using the microwindow at 2462 cm^{-1} were inconsistent with those retrieved from higher frequencies (> 2492 cm^{-1}). To remedy this likely spectroscopic issue, we have added five narrow microwindows within this 30 cm^{-1} gap to help smoothly transition between these two inconsistent microwindows. In choosing these narrow microwindows, we avoided strong lines due to $^{14}N^{14}N^{16}O$, $^{14}N^{14}N^{18}O$ and $^{12}CH_4$ so that the depth due to absorption at the line center < 7.5 % (at ACE-FTS resolution) for any remaining lines for the tangent height ranges given in Table 1. Any significant $^{18}O^{12}C^{16}O$ lines in the N_2 CIA microwindows have lower state energies of < 300 cm^{-1} and thus serve to increase the temperature-insensitive CO_2 signal. It is clear that Foucher et al. (2009, 2011) also avoided strong interfering absorption since the microwindow centered at 2462 cm^{-1} lies in the band center of the $\nu_1 + 2\nu_2$ band of $^{14}N_2^{16}O$ (which does not have a *Q* branch) and the microwindow at 2500.7 cm^{-1} lies in between the $2\nu_1$ and $\nu_1 + 2\nu_2$ bands of $^{14}N_2^{16}O$. We have modified the combined range of these twelve microwindows to span from 5 to 25 km.

For CO_2 retrieval, we have relied exclusively on $^{18}O^{12}C^{16}O$ lines to avoid any isotopic abundance inconsistencies that would arise with multiple CO_2 isotopologues. Low-*J* lines of the 20002 ← 00001 band of $^{18}O^{12}C^{16}O$ from both the *P* and *R* branches are used. Specifically, in the *P* branch, the selected lines correspond to $3 \leq J \leq 6$. From the *R* branch, *J* is in the 2 to 30 range. At $J = 30$, the lower state energy is 342.3089 cm^{-1} and thus *R* branch transitions for an initial rotation quantum number of $J \leq 30$ are weakly sensitive to temperature (Foucher, 2009). To increase the CO_2 signal at the higher altitudes, we included seven low-*J* lines in the 1371–1386 cm^{-1} region (10001 ← 00001) with microwindow settings from the ACE v3.x retrieval of $^{18}OC^{16}O$. Information on all 27 CO_2 microwindows is in Table 2. The HITRAN 2012 line intensities are from a model for both the fundamental and the first overtone bands. Because

AMTD
7, 1691–1747, 2014

the line intensity uncertainties in HITRAN 2012 are conservatively set to > 20 % for all lines mentioned above, we have compared the line intensities to measured ones (Toth, 1985; Teffo et al., 2003; Malathy Devi et al., 1984). To summarize, the agreement on the line intensities in the 10001 ← 00001 band is < 1 %, except for the weakest line at 1371.757715 cm^{-1} which differs by 1.6 %, however the semi-empirical model relies on Toth's measurements (Teffo et al., 2002) so the validation is far from independent and the measurements have never been repeated to our knowledge. For the first overtone band, the agreement is not as good with the standard deviation of relative differences being 2.5 % and the mean bias being −2.2 % (i.e. HITRAN 2012 line intensities are lower than those measured by Malathy Devi et al., 1984). The comparison with the more recent Teffo et al. (2003) measurements show a larger bias (−6 %) but reduced scatter (standard deviation of 0.8 %). The level of agreement for the first overtone band is not sufficient to allow for a measurement of CO_2 VMR with an overall uncertainty of 1–2 %. The lines from the ν_1 fundamental band are too strong to be used in the mid-troposphere.

N_2O is an important interferer in the 2485 cm^{-1} region, with transmittance between adjacent lines not reaching 100 % due to overlapping wings.

The optical thickness inside a microwindow contains contributions from lines that are up to 40 cm^{-1} outside the nearest microwindow edge (instead of 2.5 cm^{-1}) used in the ACE v3.x retrieval algorithm. This is necessary because of contributions from the far wings of strong lines such as those belonging to the ν_3 band of $^{12}C^{16}O_2$, whose line shape is sub-Lorentzian. Instead, we use a Voigt profile for all bands and discuss the impact of this assumption in Sect. 2.2.

If ignored, aerosol absorption can bias the retrieved THs by several hundred metres, rendering the simultaneously retrieved CO_2 of little scientific value. Thus, aerosol transmittance is determined empirically and used to correct transmittances in the N_2 CIA microwindows. This correction is necessary since aerosol extinction is not included in the forward model. The four spectral points (on the 0.02 cm^{-1} measurement grid) at the low frequency end of the 2637 cm^{-1} microwindow are used to determine the

AMTD
7, 1691–1747, 2014

observed total transmittance, thereby reducing the signal-to-noise ratio by a factor of ~ 2 compared to a single spectral point. Note that this microwindow covers the full TH range of the retrieval (5–25 km). Thus, it can provide the information on the aerosol contribution over this same range. The total transmittance is assumed to be the product of the aerosol transmittance and combined transmittance of the various gases. The combined gas phase transmittance is determined using simulations with the ACE forward model (Boone et al., 2005) using the atmosphere and THs retrieved with the v3.x algorithm, except that the assumed CO_2 VMR profile comes from a model which accounts for seasonal, altitudinal and latitudinal variations (Boone et al., 2013). Dividing the observed total transmittance by the modelled gaseous transmittance yields the aerosol transmittance at ~ 2637 cm^{-1}. This is assumed to be equal to the aerosol transmittance in all of the N_2 CIA microwindows (essentially 2430–2510 cm^{-1}), which appears to be a reasonable assumption if the aerosol is assumed to be pure sulfuric acid or even a 64 % by weight aqueous solution of H_2SO_4 (Nash et al., 2001), which is typical of stratospheric aerosol at 210 K (Clapp et al., 1997). Clouds are screened so the transmittance attributed to aerosol is unlikely to be due to water in solid or liquid form. Sulfate is the predominant aerosol in the stratosphere (Murphy et al., 2006) and also in the upper troposphere for cloud-free marine locations. Over land with strong convection, carbonaceous aerosols may dominate the aerosol burden in the upper troposphere (Froyd et al., 2009). We have not studied the absorption spectrum in the 2430–2640 cm^{-1} region by the latter aerosol type, but with the large number of classes of organics (Froyd et al., 2009), it is likely that some of them have spectrally-dependent absorption in this wavenumber range.

Foucher (2009) noted that there was a discontinuity at 12 km in ACE v2.2 data with regard to the altitudes, temperatures and pressures obeying hydrostatic equilibrium. This discontinuity is located at the transition between pressure and temperature (p,T) data retrieved from ACE-FTS and obtained from the assimilated meteorological fields provided by the Canadian Meteorological Center (CMC). However, we searched for such a discontinuity in the v3.x data in the lower atmosphere, and found that the

AMTD
7, 1691–1747, 2014

atmospheric p, T and altitudes obey hydrostatic equilibrium with no apparent discontinuity at the altitude of this transition.

2.2 Error budget – ACE-FTS

Rinsland et al. (2010) retrieved the partial column of CO_2 in the 7–10 km range and determined the error contribution due to several important sources such as measurement noise, temperature profile, nitrogen continuum absorption coefficients, CO_2 line intensities, aerosol absorption, CO_2 isotopologue correction, ACE-FTS ILS (instrument line shape) function, and TH shift. Foucher et al. (2009, Foucher, 2009, Foucher et al., 2011) also presented error budget information that considered measurement noise, parameter uncertainties (p and T profiles and tangent height errors), uncertainties in the VMRs of other species, as well as model and spectroscopic error. They considered the uncertainty in TH due to the uncertainty in N_2 continuum absorption coefficient spectrum and modeling error due to uncertainty in the line shape in the far wings of CO_2 and N_2O. Translating the tangent height error of 40 m to a CO_2 error using 0.09 ppm m^{-1} gives a 3.6 ppm error, which is comparable to the CO_2 uncertainty due to other dominant errors such as measurement noise in CO_2 microwindows and temperature error.

In addition to these, we consider uncertainty due to:

1. N_2-O_2 CIA and its T-dependence
2. N_2 CIA T-dependence in the 2430–2510 cm^{-1} range
3. measurement noise on the aerosol transmittances inferred from the observed spectra at 2637 cm^{-1}
4. spectral dependence of aerosol extinction in the 2430–2640 cm^{-1} region
5. unflagged cloud extinction

AMTD
7, 1691–1747, 2014

6. the sub-Lorentzian line shape of the ν_3 band of $^{12}C^{16}O_2$
7. pressure profile
8. wavelength calibration
9. CO_2 first guess profile (above and within the retrieval range)

One source of error which was not considered because it was expected to be trivial in the 5–25 km retrieval range is the uncertainty on the N_2 VMR. Rayleigh scattering was not considered since at a tangent height of 5.5 km, the transmittance is 0.9984 at our highest wavenumber of 2637 cm^{-1}. Another source of error which was neglected was H_2O continuum absorption and it warrants further investigation. There is no bias if the H_2O continuum transmittance at $\sim$ 2637 cm^{-1} is equal to its transmittance in the N_2 CIA microwindows. For a worst-case scenario of a tropical atmosphere at TH = 5.5 km, the transmittance simulated with MODTRAN5.2 (Berk et al., 2005) is 0.9671 at 2637 cm^{-1} and maximizes at 0.9859 at 2507 cm^{-1} over the N_2 CIA microwindow range (2430–2507 cm^{-1}). Another source of error relates to the modelled gas phase transmittance at $\sim$ 2637 cm^{-1}. Uncertainty in the transmittance at $\sim$ 2637 cm^{-1} due to each gaseous absorber can be implicitly taken into account in the error budget by propagating VMR and spectroscopic uncertainties through the retrieval. The uncertainty due to spectroscopic parameters of the interferers was not considered and should be considered in future work. Similarly, the uncertainties on spectroscopic parameters for the target gas ($^{18}O^{12}C^{16}O$) were also not considered, except for the line intensities, since it is expected to be the more important spectroscopic source of bias.

First, we address individual sources of error that affect retrieved CO_2 exclusively via TH uncertainty, which we group into error sources related to N_2 CIA, aerosols and finally, the sub-Lorentzian line shape of the ν_3 band of $^{12}C^{16}O_2$. Following these TH-related error sources, the remaining sources of error are then discussed in order of decreasing significance (error variance integrated over the retrieval range), although atmospheric state parameter errors are grouped together.

AMTD
7, 1691–1747, 2014

Biases in TH tend to lead to biases in CO_2 of the same sign. Because pointing errors dominate over all other error sources when tangent heights offsets are > 70 m, it is possible to empirically determine the CO_2 sensitivity from a linear regression of TH offset (relative to ACE v3.x THs) vs. CO_2 VMR using all altitudes. In doing so over a large number of occultations, we obtain a CO_2 sensitivity to tangent height offsets of 0.09 ppm m^{-1}. Using the mean TH offset profile from Fig. 4 and this sensitivity, we can empirically translate the TH bias profile to a TH-related CO_2 bias profile (Fig. 5).

Perturbing the N_2 absorption coefficient spectrum by a constant value of 0.9 %, we find an error that grows with decreasing TH. We are not sure how to interpret this other than that the retrieved THs at the top of the retrieval range might have some sensitivity to CO_2 absorption, particularly in the N_2 CIA microwindows where slope and offset terms are not fitted (see Boone et al., 2005). The resulting CO_2 uncertainty increases from ~ 2 ppm to ~ 4 ppm from the top to the bottom of the retrieval range.

By switching between the N_2 CIA T-dependence we obtained from the two best low-temperature N_2 CIA laboratory measurements (Lafferty et al., 1996; Menoux et al., 1993) to wavenumbers as high as 2600 cm^{-1}, we obtain an estimate of related uncertainty. The test was done on one occultation and the resulting TH offset profile was converted to a CO_2 error by multiplying by the sensitivity of 0.09 ppm m^{-1}. The largest error occurs at 17.5 km at the cold-point tropopause (T = 212 K) where the N_2 CIA T-dependence is extrapolated outside the range of temperatures (228–296 K) measured by Lafferty et al. (1996), but not outside the range of temperatures (193–297 K) measured by Menoux et al. (1993). In general, large errors will occur at the temperature extrema, and thus the error profile will be expected to depend on tropopause height and consequently, on latitude.

N_2-O_2 absorption coefficients in the region of the N_2 CIA fundamental band are currently not included in HITRAN 2012 (Richard et al., 2012). Using the variation of $E^{N_2}_{O_2/N_2}$ (Table 4 of Menoux et al., 1993) over six temperatures and perturbing the extreme temperature values by their uncertainties in opposite directions, we obtained

AMTD
7, 1691–1747, 2014

a slightly different best fit that ultimately translates to changes of < 0.5 ppm in retrieved CO_2 at all altitudes.

Aerosol extinction is derived from the noisy measurements. The standard deviation (σ) of the total observed transmittance for the four spectral points used for aerosol correction (see above) is a measure of the noise on the observed aerosol extinction. We propagated $+1\sigma$ observational noise at each tangent height through the retrieval and found the CO_2 sensitivity is ±0.06 ppm.

We also considered the impact of a bias in the assumed spectral dependence of aerosol extinction in the 2430–2637 cm^{-1} region, which may result if the chemical composition of the aerosols is not dominated by sulfuric acid (e.g. liquid water, ice water (Clapp et al., 1997), organic aerosol). There are a variety of different aerosol types, particularly in the troposphere, but even the mass fraction of water and its physical state (ice or liquid) are important considerations because solid state absorptions tend to be broad and the proximity of ice O-H stretch near ~ 3200 cm^{-1} to 2637 cm^{-1} could affect the slope of the aerosol extinction in the 2430–2637 cm^{-1} range (Clapp et al., 1997). The slope is currently assumed to be 0 (i.e. scaling factor of 1 between 2637 and the N_2 CIA microwindows). To consider a different scaling factor, we first convert the "observed" aerosol transmittance (see above) to an optical depth, then multiply by the scaling factor and convert back to a transmittance to account for the exponential nature of Beer's law. The CO_2 sensitivity is determined using the tangent height offsets multiplied by the CO_2 sensitivity to TH error of 0.09 ppm m^{-1}. We tested a scaling factor of 0.9 and found that this bias in TH naturally translates to a bias in retrieved CO_2. A maximum CO_2 bias of 6 ppm is estimated for the top of the retrieval range since N_2 CIA decreases exponentially with height but aerosol extinction is observed to be generally linear with altitude in the stratosphere for volcanically-unperturbed conditions (e.g. Sioris et al., 2010; Doeringer et al., 2012).

To test the effects of residual cloud contamination on the retrieval was challenging because the forward model does not simulate clouds. We made several attempts to identify occultations where clouds were barely flagged in the hope of creating a subset

AMTD
7, 1691–1747, 2014

of occultations with such borderline clouds to assess biases in TH and CO_2 due to residual cloud contamination. Some of these clouds could include volcanic aerosol plumes due to the Sarychev eruption (Doeringer et al., 2012) which affected our period of study (2009–2011). In fact, two occultations were used for case studies in Doeringer et al. (2012), namely sunsets 31 976 and 31 868, and each of these was found to have cloud tops at exactly the same tangent height as shown in that paper (e.g. their Fig. 4). This is true for both cloud products (970 and 2505.5 cm^{-1}). The best test we devised was to take occultations with the following conditions:

1. Cloud tops occur at exactly the same altitude at 970 and 2505.5 cm^{-1}.
2. Transmittance at cloud top is in the range of 0.82 to unity in cloud microwindow (a) ($tran_{cld\_top,\,a}$), where a is 970 or 2505.5 cm^{-1}.
3. Transmittance in the other microwindow at cloud top in the range of 0 to $tran_{cld\_top,\,a}$.

We collected 20 cases fulfilling the above conditions with the cloud top altitude being between 15 and 16 km. The average cloud top height was 15.53 km. The average transmittance was 0.84 and 0.85 at 970 and 2505 cm^{-1} respectively. We retrieved THs and CO_2 VMR for these cloudy cases and found the tangent heights were not biased in any detectable way relative to Fig. 3, particularly near 15 km (or below) where the bias would have been mostly likely to appear. The thin clouds are expected to affect the CO_2 retrieval only via TH biases. The residual cloud contamination is essentially nil given the current, stringent cloud flagging.

Finally, the sub-Lorentzian line shape in the ν_3 band of $^{12}C^{16}O_2$ was considered. Note that the lowest frequency in any N_2 CIA microwindow is 2429.21 cm^{-1} and the range considered outside of the microwindow is 40 cm^{-1}, so only 29 weaker lines of this ν_3 band can contribute. We find the difference in retrieved THs and CO_2 VMR is trivial if the sub-Lorentzian line shape is selected given the 40 cm^{-1} range limitation.

AMTD
7, 1691–1747, 2014

In summary, the seven theoretical sources of error which affect CO_2 via biases in retrieved TH are:

1. N_2 CIA absorption coefficient
2. N_2 CIA temperature (T) dependence
3. N_2-O_2 CIA and its T-dependence
4. measurement noise on the aerosol transmittances
5. spectral dependence of aerosol extinction in the 2430–2640 cm^{-1} region
6. residual cloud extinction
7. sub-Lorentzian line shape

The largest error source is the fifth one, by far. Error sources 1, 3, and 5–6 result in CO_2 biases whereas error sources 2 and 4 result in CO_2 retrieval error whose sign varies with altitude. Figure 5 shows errors for both empirical and theoretical approaches as negative in magnitude, since the empirical approach of determining TH errors by comparing with ACE v3.x THs has shown that THs retrieved from the N_2 CIA are biased low. The CO_2 retrieval error averaged in the vertical direction (5–25 km) is -5.0 ± 4.5 ppm ($\pm 1\sigma$) for the empirical method and -5.6 ± 1.7 ppm for the quadrature-summed individual contributions, indicating that the two methods produce similar errors and neither method shows a strong difference between the troposphere and stratosphere (> 17 km), whereas if the water vapour continuum (mentioned above) was a large source of error related to TH determination, there would be a major difference in the magnitude of errors above and below the hygropause (~ 8–12 km, depending on latitude). Note that the magnitude of the fifth source of error above, namely the spectral dependence of aerosol extinction in the 2430–2640 cm^{-1} region, was simply tested with an ad hoc and TH-independent scaling factor of 0.9 based on laboratory measurements of sulfuric acid absorption (Nash et al., 2001). Given that it is a major

AMTD
7, 1691–1747, 2014

source of error among these individual TH-related terms, and the sufficient agreement between the empirically-derived TH-related error and quadrature-summed theoretical error (within the altitudinal variability of the latter), the contribution from this error source has probably been reasonably estimated.

Biases in the CO_2 line intensities will lead to opposite biases of the same relative magnitude in retrieved CO_2 VMR. Each CO_2 microwindow targets one strong line of $^{18}O^{12}C^{16}O$. To test the sensitivity of retrieved CO_2 to uncertainties in the intensities of these targeted lines, the available measured line intensities from Malathy Devi et al. (1984) and Teffo et al. (2002) for the first overtone and the fundamental band, respectively, were used. Propagating this difference in CO_2 line intensities (measured instead of modelled) results in a 5 ppm negative bias in retrieved CO_2 VMR above 15 km and a 5–6 ppm negative bias below 15 km. The larger bias is expected below since the lines of the first overtone band ($\sim 2600\,cm^{-1}$ region) are, on the whole, more biased relative to HITRAN 2012 than the lines of the fundamental band and only the first overtone lines are used below 15 km.

To study the impact of the first guess CO_2 profile, we did three independent tests and, at each altitude, retained the largest of the three perturbations at that altitude. The first test was to switch between the default of using the first guess from the G. C. Toon model (personal communication, 2013), which will be used in ACE v4.0 retrievals (Boone et al., 2013), and using the CO_2 first guess profile used in ACE v3.x retrievals. The second test involved increasing the ACE v4.0 CO_2 profile by a factor of 1.0402 to account approximately for the atmospheric enrichment of $^{18}O^{12}C^{16}O$ due to fractionation (Wiegel et al., 2013). The third test used the VMR of $^{17}O^{12}C^{16}O$ within its retrieved range (55–96 km). These tests show a weak sensitivity of the least-squares inversion approach to the first guess of CO_2 even at the top altitude, partly because the profile above the retrieval range is scaled by a retrieved constant (Boone et al., 2005).

For each interfering molecule, we performed similar tests to the CO_2 first guess VMR tests described above. First, we positively perturb the assumed water vapour profile by its retrieval uncertainty (< 5 % below 80 km). This results in a ~ 0.1 ppm error in CO_2

AMTD
7, 1691–1747, 2014

with no obvious altitude dependence. The second test relates to isotopic variation. In the default retrieval, we assume that for each isotopologue of water vapour that its VMR is given by the VMR of the primary isotopologue (multiplied by the isotopic ratio of their natural abundances). There are no significant lines in any of our CO_2 or N_2 CIA microwindows due to $H_2^{16}O$. There are only two lines due to any water isotopologue which absorb strongly into the dry stratosphere. One belongs to HOD and the other is due to $H_2^{17}O$ and both appear in the region of the CO_2 ν_1 fundamental band. To test the impact of assuming the VMR based on $H_2^{16}O$ and the standard isotopic ratio, which essentially is testing for difference in profile shape due to atmospheric fractionation of a given isotopologue, we assume the ACE v3.x HOD VMR profile divided by its natural abundance. This is a worse case scenario since atmospheric fractionation is stronger for HOD than $H_2^{17}O$ and HOD is a minor absorber in eight other microwindow TH ranges whereas $H_2^{17}O$ absorption is negligible except for the single strong line mentioned above. Note that we attempted to retrieve HOD simultaneously but the retrieved HOD profiles were not of sufficient quality in the stratosphere, likely because the one strong line is insufficient. A maximum CO_2 sensitivity of 11 ppm is found at the top of the retrieval range where the fractionation effect is strongest, decreasing rather steadily to 0.3 ppm at 11 km when looking at an average of 10 difference profiles (to obtain a clearer H_2O fractionation signal). Thus, the impact on CO_2 of the atmospheric fractionation of water vapour is greater than that of the $H_2^{16}O$ VMR retrieval uncertainty at all altitudes. The use of the HOD VMR profile shape leads to an improved CO_2 profile shape and removes oscillations in individual CO_2 profiles that dampen with decreasing altitude. This shall be used as the first guess for water vapour in future work.

CH_4 affects both N_2 CIA and CO_2 microwindows. For CH_4, the ACE v3.x single profile retrieval uncertainty below 25 km is $\leq$3 %. Propagating this uncertainty profile (positive perturbation in the 5–75 km range) through the TH and CO_2 retrieval algorithm leads to a consistent negative bias in retrieved CO_2 of $\sim$ 0.2 ppm. According to ACE-FTS measurements, the isotopic fractionation between $^{12}CH_4$ and $^{13}CH_4$ is negligible (see also Rice et al., 2003) and the impact on retrieved CO_2 is $\sim$ 0.04 ppm.

AMTD
7, 1691–1747, 2014

Finally, for N_2O, the ACE v3.x single profile retrieval uncertainty below 25 km is ≤ 3 %. Propagating this uncertainty profile (positive perturbation over the N_2O retrieval range of 5–95 km) leads to a bias that changes sign, being negative above 11 km and positive below. The magnitude of the bias is always ≤ 0.7 ppm. The effect of fractionation of two non-primary isotopologues of N_2O (listed in Sect. 2) is considered, assuming the differences in profile shape between isotopologues are real. The CO_2 VMR sensitivity to N_2O changes appears to be via the microwindows targeting the CO_2 ν_1 first overtone band (i.e. not indirectly via TH changes).

Error in temperature translates into an air number density errors since the latter is calculated using the ideal gas law. CO_2 bias due to air density bias is expected to dominate over the CO_2 bias relating to the temperature-insensitive CO_2 absorption lines and is also larger than the CO_2 bias from the more temperature-sensitive N_2 CIA, which has an indirect effect via the tangent heights. ACE-FTS retrieved temperatures (v2.2) have been validated by Sica et al. (2008) who found differences of 2 K in the stratosphere and upper troposphere. ACE-FTS has been used in validation of temperatures from HIRDLS on Aura (Gille et al., 2008), which indicates that the ACE-FTS temperature is within 2 K between 200 and 2 hPa (12 km to upper stratosphere) and 1–2 K between 200 and 10 hPa (16–32 km). Schwartz et al. (2008) found ACE-FTS temperatures to be 1–2 K warmer in the stratosphere and 5–7 K warmer between 0.1 and 0.02 hPa (mesosphere) and 10 K warmer at 0.001 mb (~ 96 km) relative to Microwave Limb Sounder on Aura. Marshall et al. (2011) showed agreement within 3 K with Solar Occultation for Ice Experiment in the stratosphere. Garcia-Comas et al. (2012) found MIPAS and ACE-FTS temperatures to agree within 2 K up to 55 km (3 K in polar winter). They also found agreement within 3 K in the lower mesosphere, 3–4 K at 70–75 km, and within 5 K in the upper mesosphere. All of these preceding references for the quality of ACE-FTS temperatures used v2.2 data. In the only study using v3.x temperatures, Sheese et al. (2012) compared with OSIRIS and found 5 K differences in the 55 to 80 km range. Boone et al. (2013) illustrate and discuss the improvements to the temperatures retrieved from ACE-FTS between v2.2 and v3.x. Below 15 km, temperatures are

AMTD
7, 1691–1747, 2014

assumed from the analysis provided by the Canadian Meteorological Centre (CMC). According to Côté et al. (1998), these temperatures have biases of 2 K at pressures less than 500 hPa. As a worst-case scenario, we introduced a discontinuity in the temperature profile with a bias of opposite sign to the temperature bias (retrieved from ACE-FTS data) above 15 km. Specifically, the following temperature bias profile was assumed:

5–15 km: −2 K

15–55 km: +2 K

55–70 km: +3 K

70–75 km: +4 K

75–80 km: +5 K

80–85 km: +6 K

85–100 km: +10 K

Applying this assumed perturbation yields height retrieval errors of −50 m at the highest altitudes (18–22 km), and positive retrieved height errors in the range of 10–40 m below 14 km. The change of the sign of the height error relates to the opposing temperature bias (above and below 15 km) as listed above. The CO_2 retrieval bias due to this perturbed temperature profile is dominated by the air density perturbation particularly at the lowest temperatures (i.e. tropopause) where the relative change in air density of a +2 K perturbation will be greatest. The sensitivity of CO_2 to temperature biases is reduced by the fact that there are cancelling biases due to air density biases and TH-related biases (via N_2 CIA). The CO_2 retrieval bias reaches a local maximum in magnitude of +1.2 % at 16 km and this is the only altitude where the bias is significant relative to the retrieval uncertainty. There is a maximum at 5 km of +1.4 %.

AMTD
7, 1691–1747, 2014

Errors in pressure can impact the CO_2 retrieval algorithm because of pressure broadening of absorption lines. Below 15 km, the pressure assumed in the CO_2 retrieval comes from the CMC analysis (Côté et al., 1998). To obtain a reasonable pressure uncertainty, we took the geopotential height bias of the forecast at 100 hPa (~ 16 km) of 25 m (Qaddouri and Lee, 2011) and converted this to a relative error of ~ 0.16 % and assumed that this corresponds to the relative pressure bias. Below this altitude, the relative geopotential height biases are actually smaller. We applied this ~ 0.16 % pressure bias to all altitudes up to 150 km). The resulting impact on CO_2 VMR was rather random, with a standard deviation of 0.99 ppm and a mean bias over height of 0.08 ppm.

To test the effect of the half-width of the instrument function, we independently changed each of the three parameters in the empirical expression used by Boone et al. (2013) for self-apodization by 2.86 % based on worst-case spectral resolution variability determined at four wavenumbers along the ACE-FTS spectral range (Châteauneuf et al., 2005). CO_2 VMR was sensitive mostly to the third parameter (differences of up to 1.3 ppm), with the sensitivity decreasing slightly from this upper limit at the top of the retrieval range where the width of the ILS exceeds the widths of the absorption lines to a relatively constant value of 1.1 ppm below 13 km where the widths of the absorption lines can exceed the ILS width.

To test the sensitivity of CO_2 to observation noise, we increased the noise in existing real ACE-FTS data without any TH-dependence by adding uniform noise which is 1/454 of the signal. In combination with the existing real noise which is 1/400 of the signal (Châteauneuf et al., 2005), we estimate that the final SNR would be reduced to approximately 300. We find that changing the SNR from 400 to 300 made a difference of up to 1.6 ppm in the retrieved CO_2 with the greatest impact at the top of the profile, where the CO_2 lines are less deep, and also below 7 km, where absorption saturation leads to smaller transmittance signal changes per unit change in CO_2 VMR.

Regarding the wavelength calibration, we tested the impact of changing the first guess of the wavelength calibration by a thirtieth of the ACE-FTS spectral resolution.

AMTD
7, 1691–1747, 2014

Larger perturbations are unrealistic given the accuracy of the wavelength calibration and the accuracy of the spectroscopic line parameters that are used. The retrieval is not expected to have much sensitivity to the first guess of the wavelength calibration because the wavelength calibration is redetermined during the retrieval but since it is an input of the retrieval, we tested it and found that the retrieved CO_2 VMR can change by 0.2 ppm.

With respect to the overall error budget, it was necessary to avoid double-counting certain sources of error. These sources of error are the empirically-derived TH-related error and the observational noise in the 2637 cm^{-1} microwindow. For the former, we preferred the theoretically-derived TH-related error profile because the empirically-derived one is based on 129 occultations and the sample sizes are very small at the lowest THs (because sunset and sunrise occultations stop and start, respectively, at the top of optically-thick clouds). An additional error contribution was added in quadrature into the overall error budget to account for the uncertainty of the relative isotopic fraction of $^{18}O^{12}C^{16}O$ caused by its atmospheric variability. $^{18}O^{12}C^{16}O$ is enriched in the troposphere by a relatively constant value of ~ 4.1 % (Kawagucci et al., 2008) relative to standard mean ocean water (SMOW), which is the standard used in HITRAN2012 for CO_2 isotopic abundances. This factor can be taken into account except that it varies with the abundance of O^1D and thus, particularly in the stratosphere, it is a function of altitude, latitude, season and proximity to the polar vortex. In the stratosphere, using data from Kawagucci et al. (2008), we calculated that the mean and standard deviation of this enrichment factor is 4.314 ± 0.227 %. We have taken this measure of variability in order to account for this uncertainty source when reporting total CO_2 error based on $^{18}O^{12}C^{16}O$ measurements for all altitudes > 10 km and assume no related error in the troposphere. In the stratosphere, the uncertainty propagated to total CO_2 is 0.218 ppm. The median absolute value of latitude for ACE-FTS CO_2 data is 61°, where the tropopause is at 10 km in the Southern Hemisphere and 9 km in the Northern Hemisphere (SPARC, 1998).

AMTD
7, 1691–1747, 2014

The assumed water vapour profile is the dominant source of error at the top of the retrieval range. The contribution of aerosol extinction relative to N_2 CIA is a maximum in the lower stratosphere, near the Junge layer and this source of error dominates in the 18–21 km range. $^{18}O^{12}C^{16}O$ line intensity uncertainties dominate at all other altitudes, except at the temperature extremes, where the T-dependence of the N_2 CIA becomes dominant. Figure 6 shows the total error ranges between 6 and 11 ppm and many sources of error could be reduced with improved knowledge of forward model inputs.

2.3 Error budget – CASS

CASS is a proposed mission involving an FTS similar to the one used in the ACE mission, but accompanied by solar imagers with the potential to independently provide improved pointing knowledge (Melo et al., 2013). Thus the error budget for CASS is different than the error budget for ACE with respect to uncertainties in TH and also in the temperature profile.

The CASS-FTS total CO_2 uncertainty (~ 7–8 ppm) is slightly lower than for ACE at most altitudes, but the magnitude depends strongly on the assumed tangent height uncertainty (Fig. 7). If the CASS imagers (or other methods) can achieve tangent height uncertainties significantly better than 50 m, this will yield lower uncertainties in the retrieved CO_2 VMR profile.

Temperature target accuracy for CASS-FTS is 2 K between 10–50 km and 4 K between 50–100 km and 5–10 km. Propagation of this temperature bias leads to a CO_2 bias of +1.7 % at 5 km, decreasing to 1 % at 6 km, and < 1 % below 8 km. Temperature is only a significant source of error at 9 km relative to retrieval uncertainties. The CASS-FTS temperature target accuracy is sufficient to achieve the CO_2 target accuracy in the absence of other error sources.

AMTD
7, 1691–1747, 2014

3 Results

Using the improved temperature dependence of the N_2 CIA and accounting for aerosol extinction in the N_2 CIA microwindows, we found improved pointing accuracy relative to using the temperature dependence of Foucher (2009) by comparison with the ACE-FTS v3.x tangent heights. Using the N_2 CIA temperature dependence of Foucher (2009) leads to a low bias of 200 m relative to ACE-FTS v3.x tangent heights. The impact of neglecting the aerosol extinction in the N_2 CIA microwindows introduces altitude-dependent TH offsets that become very apparent if the TH retrieval spans a sufficient range (5–25 km). This is discussed in Sect. 4.

Boone et al. (2005) report a residual ~+100 m difference in THs retrieved independently using $^{18}O^{12}C^{16}O$ and $^{16}O^{12}C^{16}O$ microwindows with the ACE v2.2 retrieval software, after correcting for an apparent high bias of 3.5 % in the VMR of the rarer isotopologue. This correction factor was increased to +4.3 %, which is a more representative value for the isotopic enrichment of $^{18}O^{12}C^{16}O$ in the stratosphere (Wiegel et al., 2013; Kawagucci et al., 2008) for ACE v3.x retrievals. Thus, ACE v3.x THs would be expected to have this high bias reduced to +43 m assuming the latter correcting factor. Thus, the −61 m bias vs. ACE v3.x THs shown in Fig. 4 is reduced to −18 m when the ACEv3.x TH high bias due to CO_2 isotopic inconsistencies is considered.

Using the HITRAN 2012 linelist for the retrieval of THs using the ACE v3.x software leads to a decrease in THs of 62 ± 8 m in the 15–25 km range relative to the use of the default linelist which is an updated version of HITRAN 2004. Similarly, below 15 km where $^{18}O^{12}C^{16}O$ lines are exclusively used for ACE v3.x TH retrieval (Boone et al., 2013), a larger TH decrease of 118 ± 45 m is observed.

Finally, the ACE v3.x THs are biased low because of the low-biased CO_2 VMR profile due to the underestimated growth rate of 1.50155 ppm yr^{-1} of CO_2 (Boone et al., 2005). To study this effect, we have used a CO_2 model which captures the latitudinal, seasonal, and long-term variation of CO_2 (G. C. Toon, personal communication, 2013). Foucher et al. (2009) note that the seasonal cycle of CO_2 in the troposphere could

AMTD
7, 1691–1747, 2014

lead to seasonally-varying biases in the mid-tropospheric THs. By replacing the default CO_2 VMR profile with profiles from the Toon CO_2 model for Northern Hemisphere mid-latitude April and October, we find that the THs above 10 km are not sensitive to the seasonal cycle of CO_2, consistent with Foucher et al. (2009), but exhibit sensitivity to the low bias in assumed CO_2 VMR due to the underestimated growth rate. The bias in THs due to assumed CO_2 is $+40 \pm 20$ m at 25 km, partly due to the assumption of a constant VMR profile in the stratosphere (20–60 km), whereas Toon's model shows a 4.5 ppmv increase from 60 km down to 20 km. This bias in TH grows steadily to ~+110 m at the tropopause (10 km). In summary, two changes have been included to the ACE v3.x TH retrieval to make the resulting THs more accurate:

1. spectroscopic update
2. assumed CO_2 VMR profile

The two changes have opposite effects that are of the same magnitude both above and below 15 km. Thus the ACE v3.x tangent heights are essentially unchanged within 50 metres (for altitude above 7 km) when both of these effects are taken into account simultaneously.

3.1 Post-processing data filters

CO_2 retrieved from ACE-FTS is generally reliable. Figure 8 shows a three year (2009–2011) median profile from cloud-free data. However, on rare occasions the retrieved profile can be implausible. This may be a result of the aerosol extinction correction which may fail as transmittance at 2637 cm^{-1} approaches nil at low tangent heights. There may be other causes as well (e.g. missing or corrupt data). Thus from any of the results shown here, we exclude a small fraction of points with negative CO_2 VMR. Also, we remove data points where the CO_2 VMR uncertainty is reported as 0.00 or > 1 (i.e. uncertainty calculation failed). Finally, we removed points with VMR > 0.00062 given Fig. 9. We have been very conservative so as to not remove any high CO_2 values that could result from rapid lofting of enhancements at the surface to heights of > 5 km.

AMTD
7, 1691–1747, 2014

3.2 Validation of CO_2 profiles vs. latitude with in-situ data

We validate by latitude and altitude with in situ data from airborne sensors. Using only clear-sky data, certain latitude regions provided few validation opportunities, especially in the troposphere. Therefore, we attempted to expand the number and spatial coverage of validation opportunities by including a subset of data which was flagged as cloudy at 2505.5 cm^{-1} but not at 970 cm^{-1}. These are not tropospheric clouds, but rather polar, lower stratospheric aerosols that occur in all seasons. Most of these aerosols likely include water-ice which absorbs the 2100–3600 cm^{-1} region (Clapp et al., 1997) and forms at temperatures below 210 K (depending on mass fraction of sulphate relative to water-ice). Based on the 2505.5 cm^{-1} cloud flag, these aerosols are observed to exist in a narrow layer between 13 and 15 km, with greatest frequency near 60–66° latitude. We retrieved CO_2 VMR from all occultations belonging to this subset of data using v3.0 inputs for 2009 and up to September 2010 and v3.5 inputs after September 2010 until the end of 2011. This was necessary since v3.0 data is not valid beyond September 2010 (Boone et al., 2013). The retrieved CO_2 profiles show a high bias of 8 ppm at 13.5 and 7 ppm at 14.5 km, and no significant impact on this 21 month median profile at all other altitudes (not shown). We validate this "cloudy" dataset as well, which greatly improves our ability to detect latitudinal biases.

Longitudinal variations are not validated. The annual growth (Fig. 10) validates the stability of the retrieved CO_2 vs. time. Furthermore, it demonstrates that small increases of 2–3 ppm yr^{-1} are detectable when averaging vertically over the lower stratosphere. Data from the following in-situ sources are used: HIPPO (HIAPER Pole-to-Pole Observations) (Wofsy et al., 2011), CONTRAIL (Comprehensive Observation Network for Trace gases by Airline) (Machida et al., 2008), and CARIBIC (Civil Aircraft for the Regular Investigation of the atmosphere Based on an Instrument Container) (Schuck et al., 2009).

Multiple instruments on the five HIPPO measurement campaigns were used to measure CO_2 (Wofsy et al., 2011); however, in this work we only use the CO2.X data

AMTD
7, 1691–1747, 2014

product. CO2.X data is primarily made up of measurements from the Quantum Cascade Laser Spectrometer, with gap filling from the Observations of the Middle Stratosphere instrument (Daube et al., 2002), and times of potential problems and uncertainty estimates informed by the AO2 (Atmospheric Oxygen) instrument and the two flask samplers. The HIPPO dataset covers 9 of 12 calendar months with good latitudinal and altitudinal coverage.

We used CONTRAIL measurements made by the Continuous CO_2 Measuring Equipment (CME) carried aboard commercial passenger aircraft. The CONTRAIL CO_2 measurements used in this work were made with a non-dispersive infrared (NDIR) gas analyzer (Licor 840).

For CARIBIC, air samples are collected from commercial aircraft flights using an automated system. The samples obtained are analyzed in a laboratory using a gas chromatograph equipped with a flame ionization detector, for which CO_2 is converted to CH_4 using a nickel catalyst prior to analysis (Schuck et al., 2009).

ACE-FTS single profile measurements are compared with monthly 10° zonal means of in-situ data in 1 km vertical increments. Validation opportunities cover the 5.075–13.999 km range of ACE altitudes and years 2009 to 2011. If more than one correlative instrument provides a validation opportunity in the same year and month, latitude band, and height interval, then we avoid duplication by selecting only data from one correlative instrument, in the following priority sequence: HIPPO, CONTRAIL, and CARIBIC. The ACE-FTS retrieved VMR of $^{18}O^{12}C^{16}O$ is converted to total CO_2 (i.e. all isotopologues) by dividing by its SMOW isotopic abundance fraction. In the troposphere ($z \leq 10$ km), we divide by 1.0402 (Wiegel et al., 2013) which accounts for the difference between the SMOW standard and the more appropriate Pee Dee Belemnite (PDB) standard. For the stratosphere ($z > 10$ km), we divide the ACE total CO_2 VMR by 1.04314 instead to account for a minor contribution from atmospheric fractionation in the stratosphere. Post-processing data filters (see Sect. 3.1) are applied.

The global median bias including all latitudes and altitudes is -1.7 ± 0.4 ppm (± standard error, SE). Figure 11 shows that between 7 and 12 km, the only significant biases

AMTD
7, 1691–1747, 2014

occur at 8 km (6.2 ± 2.3 ppm) and negative biases of 2.3 ± 0.5 ppm over the 9–12 km range. At 5–6 km, there are too few coincidences ($N \leq 13$) to determine whether the bias is statistically significant. The negative bias in the 9–12 km region is driven by known negative CO_2 bias of 5 ± 3 ppm due to tangent height offsets (Fig. 5). At 13 km, the positive bias of 7 ± 1 ppm (±SE) is due to aerosol-related biases in the "cloudy" cases. The cause of the positive bias at 8 km is not known, but the bias is < 2 % of CO_2.

Figure 12 shows the validation by latitude band. Four latitude bands also show a negative bias of ∼ 5 ± 4 ppm, whereas at southern high latitudes, a slight positive bias (1.9 ± 1.9 ppm) is found. Again, the sign and magnitude of the negative bias at most latitudes is expected. The cause of the positive bias at southern high latitudes is unknown but, again, it is < 1 % of CO_2.

We focus on the latitude bands with the most validation opportunities (Fig. 12), namely high and mid-latitudes, in order to examine the altitude dependence of any latitudinal bias. At southern mid-latitudes, the validation indicates significant negative biases only at 10 to 12 km of 5 ± 3 ($N = 28$), 4 ± 2 ppm ($N = 40$), and 6 ± 4 ppm ($N = 32$), respectively (Fig. 13). The sign and magnitude are expected based on tangent height bias. At 13 km, the sign and magnitude of the positive bias of 3 ± 3 ppm is expected from aerosol-related biases in the "cloudy" subset (∼ 8.5 ppm), offset by a negative offset of 5 ppm from low-biased THs. At all other altitudes, the biases are statistically insignificant.

For Northern Hemisphere mid-latitudes, samples sizes are small ($N < 20$) below 9 km. The bias is consistent with southern mid-latitudes in the 9–12 km range. At 13 km, given that the validation opportunities are almost entirely for "cloudy" cases, the +8.5 ppm expected bias due to aerosols (discussed above) is added on a negative bias of ∼ 5 ppm from tangent heights. Thus a positive bias of 3.5 ppm is expected, which agrees with the observed 3.4 ± 2.7 ppm bias (± SE).

For northern high latitudes, the validation sample size is small ($N \leq 12$) below 9 km. The sample sizes are adequate ($N \geq 20$) in the 9–12 km range. Between 10 and 12 km,

AMTD
7, 1691–1747, 2014

a negative bias of 1 ± 1 ppm is observed, similar to mid-latitudes and at 13 km, a positive bias of 11 ± 2 ppm is found, slightly larger than other latitude bands and caused by "cloudy" points. The high bias (∼ 1 %) at northern high latitudes at 9 km largely determines the global bias at 8–9 km (Fig. 11). As mentioned, its cause is not understood.

At southern high latitudes, the sample size is sufficient, only at 12–13 km. At 12 km, the bias is not significant, whereas at 13 km, a positive bias of 5 ± 3 ppm is found, similar to other latitudes, and almost entirely due to the positive bias relating to lower stratospheric aerosols.

4 Conclusion and future work

There are four major advances in this work over the previous work (e.g. Foucher et al., 2011 and references therein):

1. the transmittance due to sulfate aerosol is considered
2. significantly improved temperature-dependence of N_2 CIA
3. addition of several narrow N_2 CIA microwindows to improve retrieval of the TH vector
4. no dependence of the retrievals on a chemistry-transport model via the a priori

If sulfate aerosol transmittance is neglected the TH offsets relative to ACE v3.x have a TH-dependence. There is a gradient of several hundred metres in these TH offsets because the contribution of aerosol absorption relative to N_2 CIA grows with increasing TH. N_2 CIA decreases quadratically with decreasing air density (i.e. increasing TH) due to the binary nature of the absorption whereas aerosol absorption is expected to decrease more linearly as aerosol extinction is proportional to air density for background cases. Foucher (2009) found such a TH offset gradient as well and used averaged vertical profiles of TH offsets to correct for their neglect of aerosol absorption. Their

AMTD
7, 1691–1747, 2014

method is susceptible to aerosol variability which can be significant given recent volcanic activity (Sioris et al., 2010; Doeringer et al., 2011).

A consistent spectrum of the temperature-dependence coefficient for the N_2 CIA is found between the measurements of Lafferty et al. (1996) and Menoux et al. (1993). The use of Hartmann's temperature-dependence led to THs that were offset by > 1 km from those obtained using the ACE v3.x retrieval. This necessitated the re-analysis of Lafferty et al. (1996) data to obtain a much improved temperature dependence spectrum (Foucher, 2009). Using Foucher's temperature dependence, we obtain a mean TH offset of −200 m relative to ACE v3.x with no significant vertical gradient, whereas using the temperature dependence determined here, the TH offset is further reduced, typically to less than 100 m.

The retrievals shown in Foucher et al. (2009, 2011) show a strong dependence on the a priori particularly above 20 km, which, in turn, leads to reduced variability in retrieved CO_2 compared with our work. Specifically, if we use their small set of N_2 CIA microwindows, we also find a kink in the retrieved CO_2 profile near 16 km (Foucher et al., 2011) which we find to be related to inconsistencies between N_2 CIA microwindows. This kink is damped in their retrieval by constraining CO_2 to the a priori. We find a much larger anomaly appears at the same altitude in our retrieved CO_2 profiles and the vertical profile of TH offsets (averaged over a large number of occultations). Using an improved and more extensive set of N_2 CIA microwindows (Table 1), significant kinks are largely reduced.

Future endeavours should include the simultaneous retrieval of the B_0 and β_0 parameters from the measurements of Lafferty et al. (1996). Ideally the simultaneous retrieval of these spectral quantities could be performed on a finer grid than 5 cm^{-1}. Then, the CO_2 retrieval could be repeated using N_2 CIA parameters on a finer grid. This may capture some of the weak, fine structure in the N_2 CIA that has been the subject of much investigation (e.g. Lafferty et al., 1996; Moreau, 1999).

Microwindows could be added to retrieve non-primary isotopologues of interfering species simultaneously and accurately. There are ∼ 500 000 available CO_2 lines in

AMTD
7, 1691–1747, 2014

HITRAN 2012. Additional microwindows for CO_2 should be sought to improve detection in the upper troposphere where CO_2 retrieval uncertainties grow exponentially. For example, the retrieval uncertainty, which is a statistical output of the least-squares retrieval algorithm, can be as small as 1.0 ppm at 10 km (Antarctic stratosphere), whereas at 6 and 5 km, the minimum statistical uncertainty in the cloud-free dataset grows to 5 and 11 ppm, respectively.

Next, we discuss whether the ACE-FTS CO_2 dataset presented here is sufficiently precise to detect natural variability on monthly and annual time scales and on global horizontal scale and within a 5 km range (7–12 km) in the upper troposphere and lower stratosphere). Detecting CO_2 variations over shorter spatial and temporal scales becomes more challenging. The small-scale variability is determined by looking at the variability about the monthly mean, calculated in 10° latitude bins and 1 km vertical increments. Using the HIPPO dataset, natural small-scale variability reaches a maximum of 4.3 ppm (standard deviation, $N = 64$) at 5.5 km at 85° N in July 2011. However, monthly-scale temporal variability can be determined by looking at variations between consecutive months (for the same altitude and latitude). At an annual time scale, time-dependent measurement biases (i.e. drifts) are much smaller than the annual increase in CO_2. Natural year-to-year variations are small, on the order of 2.5 ppm yr^{-1}, but ACE-FTS CO_2 has a high degree of temporal stability and can be used to detect this level of change. This is possible due to the self-calibrating nature of the solar occultation measurements.

As discussed in Sect. 3.2 (Fig. 11), biases vs. altitude between 7 and 12 km are on the order of 9 ppm. Natural variations in this altitude range can reach 8 ppm in April 2010 at 65° N (according to HIPPO data). The vertical gradient in the boreal early spring is mostly due to the strong seasonal cycle in the Arctic mid-troposphere.

Biases vs. latitude (maximum bias difference of 11.1 ppm between tropics and the southern polar region shown in Fig. 12) exceed the natural latitude gradient of 9.2 ppm at 5.5 km in April 2010 (maximum and minimum at 85° N and 65° S, respectively, according to HIPPO). Nevertheless, ACE-FTS CO_2 bias differences between southern

AMTD
7, 1691–1747, 2014

high-latitudes and northern mid-latitudes are on the order of 5 ppm at 12 km (Fig. 13). According to in-situ observations (Fig. 14, left panel), the latitude gradient between 45° N and 65° S at 10 km in boreal spring is 6 ppm. Figure 14 shows the 6 and 4 ppm gradient at 9.5 and 10.5 km, respectively using differences between CONTRAIL and HIPPO observations from these two latitude bands. According to the ACE-FTS retrievals, the gradients are of 5, 6, 4, and 1 ppm at 9.5, 10.5, 11.5, 12.5 km. The decreasing latitudinal gradient with height is expected at 12.5 km because both latitude bands are in the stratosphere at this altitude, where the gradients are smaller because they are not as sensitive to local sources and sinks as the upper troposphere. This latitudinal gradient disappears toward the end of boreal summer at 10 km due to the strong biospheric uptake at northern extratropical latitudes (Fig. 14, right panel). Thus the latitudinal gradient has a seasonal variation. The low CO_2 bias of ACE-FTS due to tangent height offsets also appears in Fig. 14. Also, the consistency between boreal summer and spring CO_2 VMR near the tropopause in the ACE-FTS data is encouraging.

The vast majority of ACE-FTS CO_2 profiles which extend below 6.5 km are located in the Antarctic, which is a region of no flux, and the Southern ocean, which has one of the smallest posterior errors of any region (Pak and Prather, 2001; Baker et al., 2006). This presents a challenge for constraining fluxes from satellite-based upper tropospheric profile measurements. The present scientific value of the ACE-FTS CO_2 data lies mostly in providing continuous global monitoring of the vertical profile in the upper troposphere and lower stratosphere with good temporal stability and small retrieval uncertainties in the stratosphere as expected from a solar occultation FTS. Taking annual means further magnifies the difference in uncertainties between the troposphere and stratosphere because clouds limit the fraction of occultations which provide tropospheric data.

AMTD
7, 1691–1747, 2014

Acknowledgements. This work was supported by the Canadian Space Agency through a memorandum of understanding with Environment Canada. We acknowledge Laurence Rothman (Harvard-Smithsonian Center for Astrophysics) for guidance in converting between line intensities reported with different units. Lin Huang (Environment Canada) helped us to understand the different standards used in isotopic measurements. Toshinobu Machida (National Institute for Environmental Studies, Japan), Hidekazu Matsueda, and Yousuke Sawa (both at Meteorological Research Institute, Japan) are acknowledged for providing the CONTRAIL data. We acknowledge Britt Stephens (National Center for Atmospheric Research) for providing guiding comments regarding HIPPO CO_2 data and Steve Wofsy as HIPPO lead principal investigator. We thank Carl Brenninkmeijer for his suggestions on an earlier draft of this manuscript and, together with Tanja Schuck (both at Max Planck Institute for Chemistry), for providing the CARIBIC data.

References

Baker, D. F., Law, R. M., Gurney, K. R., Rayner, P., Peylin, P., Denning, A. S., Bousquet, P., Bruhwiler, L., Chen, Y.-H., Ciais, P., Fung, I. Y., Heimann, M.,John, J., Maki, T., Maksyutov, S., Masarie, K., Prather, M., Pak, B., Taguchi, S., and Zhu, Z.: TransCom 3 inversion intercomparison: impact of transport model errors on the interannual variability of regional CO_2 fluxes, 1988–2003, Global Biogeochem. Cy., 20, GB1002, doi:10.1029/2004GB002439, 2006.

AMTD

7, 1691–1747, 2014

Baranov, Y. I., Buryak, I. A., Lokshtanov, S. E., Lukyanchenko, V. A., and Vigasin, A. A.: H_2O-N_2 collision-induced absorption band intensity in the region of the N_2 fundamental ab initio investigation of its temperature dependence, Philos. T. Roy. Soc. A, 370, 2691–2709, 2012.

Beagley, S. R., Boone, C. D., Fomichev, V. I., Jin, J. J., Semeniuk, K., McConnell, J. C., and Bernath, P. F.: First multi-year occultation observations of CO_2 in the MLT by ACE satellite: observations and analysis using the extended CMAM, Atmos. Chem. Phys., 10, 1133–1153, doi:10.5194/acp-10-1133-2010, 2010.

Berk, A., Anderson, G. P., Acharya, P. K., Bernstein, L. S., Muratov, L., Lee, J., Fox, M., Adler-Golden, S. M., Chetwynd, J. H., Hoke, M. L., Lockwood, R. B., Gardner, J. A., Cooley, T. W., Borel, C. C., Lewis, P. E.: MODTRAN™ 5, a reformulated atmospheric band model with auxiliary species and practical multiple scattering options: update, Proc. SPIE, 5806, 662–667, 2005.

Boone, C. D., Nassar, R., Walker, K. A., Rochon, Y., McLeod, S. D., Rinsland, C. P., and Bernath, P. F.: Retrievals for the atmospheric chemistry experiment Fourier-transform spectrometer, Appl. Optics, 44, 7218–7231, 2005.

Boone, C. D., Walker, K. A., and Bernath, P. F.: Version 3 retrievals for the Atmospheric Chemistry Experiment Fourier Transform Spectrometer (ACE-FTS), in: The Atmospheric Chemistry Experiment ACE at 10, A Solar Occultation Anthology, edited by: Bernath, P. F., A., Deepak Publishing, Hampton, VA, 103–127, 2013.

Châteauneuf, F., Soucy, M.-A., and Fortin, S.: ACE-FTS instrument: after two years on-orbit, Proc. SPIE, 5883, doi:10.1117/12.626663, 2005.

Clapp, M. L., Niedziela, R. F., Richwine, L. J., Dransfield, T., and Miller, R. E., Worsnop, D. R.: Infrared spectroscopy of sulfuric acid/water aerosols: freezing characteristics, J. Geophys. Res., 102, 8899–8907, 1997.

Côté, J., Desmarais, J.-G., Gravel, S., Méthot, A., Patoine, A., Roch, M., and Staniforth, A.: The Operational CMC–MRB Global Environmental Multiscale (GEM) model, Part II: Results, Mon. Weather Rev., 126, 1397–1418, 1998.

Daube, B. C., Boering, K. A., Andrews, A. E., and Wofsy, S. C.: A high-precision fast-response airborne CO_2 analyzer for in situ sampling from the surface to the middle stratosphere, J. Atmos. Oceanic Technol., 19, 1532–1543, 2002.

AMTD
7, 1691–1747, 2014

Doeringer, D., Eldering, A., Boone, C. D., González Abad, G., and Bernath, P. F.: Observation of sulfate aerosols and SO_2 from the Sarychev volcanic eruption using data from the Atmospheric Chemistry Experiment (ACE), J. Geophys. Res., 117, D03203, doi:10.1029/2011JD016556, 2012.

Emmert, J. T., Stevens, M. H., Bernath, P. F., Drob, D. P., and Boone, C. D.: Observations of increasing carbon dioxide concentration in Earth's thermosphere, Nat. Geosci., 5, 868–871, 2012.

Fischer, H., Birk, M., Blom, C., Carli, B., Carlotti, M., von Clarmann, T., Delbouille, L., Dudhia, A., Ehhalt, D., Endemann, M., Flaud, J. M., Gessner, R., Kleinert, A., Koopman, R., Langen, J., López-Puertas, M., Mosner, P., Nett, H., Oelhaf, H., Perron, G., Remedios, J., Ridolfi, M., Stiller, G., and Zander, R.: MIPAS: an instrument for atmospheric and climate research, Atmos. Chem. Phys., 8, 2151–2188, doi:10.5194/acp-8-2151-2008, 2008.

Foucher, P. Y., Chédin, A., Dufour, G., Capelle, V., Boone, C. D., and Bernath, P.: Technical Note: Feasibility of CO_2 profile retrieval from limb viewing solar occultation made by the ACE-FTS instrument, Atmos. Chem. Phys., 9, 2873–2890, doi:10.5194/acp-9-2873-2009, 2009.

Foucher, P. Y., Chédin, A., Armante, R., Boone, C., Crevoisier, C., and Bernath, P.: Carbon dioxide atmospheric vertical profiles retrieved from space observation using ACE-FTS solar occultation instrument, Atmos. Chem. Phys., 11, 2455–2470, doi:10.5194/acp-11-2455-2011, 2011.

Foucher, P. Y.: Détermination de profils verticaux de concentration en CO_2 atmosphérique à partir d'observations spatiales. Application aux données en occultation solaire de l'instrument ACE-FTS sur SCISAT 1. PhD thesis, Université de Paris VI, 198 pp., 2009.

Froyd, K. D., Murphy, D. M., Sanford, T. J., Thomson, D. S., Wilson, J. C., Pfister, L., and Lait, L.: Aerosol composition of the tropical upper troposphere, Atmos. Chem. Phys., 9, 4363–4385, doi:10.5194/acp-9-4363-2009, 2009.

García-Comas, M., Funke, B., López-Puertas, M., Bermejo-Pantaleón, D., Glatthor, N., von Clarmann, T., Stiller, G., Grabowski, U., Boone, C. D., French, W. J. R., Leblanc, T., López-González, M. J., and Schwartz, M. J.: On the quality of MIPAS kinetic temperature in the middle atmosphere, Atmos. Chem. Phys., 12, 6009–6039, doi:10.5194/acp-12-6009-2012, 2012.

AMTD
7, 1691–1747, 2014

Gille, J., Barnett, J., Arter, P., Barker, M., Bernath, P., Boone, C., Cavanaugh, C., Chow, J., Coffey, M., Craft, J., Craig, C., Dials, M., Dean, V., Eden, T., Edwards, D. P., Francis, G., Halvorson, C., Harvey, L., Hepplewhite, C., Khosravi, R., Kinnison, D., Krinsky, C., Lambert, A., Lee, H., Lyjak, L., Loh, J., Mankin, W., Massie, S., McInerney, J., Moorhouse, J., Nardi, B., Packman, D., Randall, C., Reburn, J., Rudolf, W., Schwartz, M., Serafin, J., Stone, K., Torpy, B., Walker, K., Waterfall, A., Watkins, R., Whitney, J., Woodard, D., and Young, G.: High resolution dynamics limb sounder: experiment overview, recovery and validation of initial temperature data, J. Geophys. Res., 113, D16S43, doi:10.1029/2007JD008824, 2008.

Goldman, A., Tipping, R. H., Ma, Q., Boone, C. D., Bernath, P. F., Demoulin, P., Hase, F., Schneider, M., Hannigan, J. W., Coffey, M. T., Rinsland, C. P.: On the line parameters for the $X^1\Sigma^+ g(1\text{–}0)$ infrared quadrupolar transitions of $^{14}N_2$, J. Quant. Spectrosc. Ra., 103, 168–174, 2007.

Hofmann, D. J., Butler, J. H., and Tans, P. P.: A new look at atmospheric carbon dioxide, Atmos. Environ., 43, 2084–2086, 2009.

Kawagucci, S., Tsunogai, U., Kudo, S., Nakagawa, F., Honda, H., Aoki, S., Nakazawa, T., Tsutsumi, M., and Gamo, T.: Long-term observation of mass-independent oxygen isotope anomaly in stratospheric CO_2, Atmos. Chem. Phys., 8, 6189–6197, doi:10.5194/acp-8-6189-2008, 2008.

Lafferty, W. J., Solodov, A. M., Weber, A., Olson, W. B., and Hartmann, J.-M.: Infrared collision-induced absorption by N_2 near 4.3 µm for atmospheric applications: measurements and empirical modeling, Appl. Optics, 35, 5911–5917, 1996.

Machida, T., Matsueda, H., Sawa, Y., Nakagawa, Y., Hirotani, K., Kondo, N., Goto, K., Ishikawa, K., Nakazawa, T., and Ogawa, T.: Worldwide measurements of atmospheric CO_2 and other trace gas species using commercial airlines, J. Atmos. Ocean. Tech., 25, 1744–1754, doi:10.1175/2008JTECHA1082.1, 2008.

Malathy Devi, V., Rinsland, C. P., and Benner, D. C.: Absolute intensity measurements of CO_2 bands in the 2395–2680 cm^{-1} region, Appl. Optics, 23, 4067–4075, 1984.

Marshall, B. T., Deaver, L. E., Thompson, R. E., Gordley, L. L., McHugh, M. J., Hervig, M. E., and Russell III, J. M.: Retrieval of temperature and pressure using broadband solar occultation: SOFIE approach and results, Atmos. Meas. Tech., 4, 893–907, doi:10.5194/amt-4-893-2011, 2011.

AMTD
7, 1691–1747, 2014

Melo, S. M. L., Walker, K. A., and Degenstein, D.: The Chemical and Aerosol Sounding Satellite (CASS) mission as a solution for global climate quality atmospheric composition measurements, in: The Atmospheric Chemistry Experiment ACE at 10: A Solar Occultation Anthology, edited by: Bernath, P. F., A. Deepak Publishing, Hampton, VA, USA, 323–330, 2013.

Menoux, V., Le Doucen, R., Boulet, C., Roblin, A., and Bouchardy, A. M.: Collision-induced absorption in the fundamental band of N_2: temperature dependence of the absorption for N_2-N_2 and N_2-O_2 pairs, Appl. Optics, 32, 263–268, 1993.

Murphy, D. M., Cziczo, D. J., Froyd, K. D., Hudson, P. K., Matthew, B. M., Middlebrook, A. M., Peltier, R. E., Sullivan, A., Thomson, D. S., and Weber, R. J.: Single-particle mass spectrometry of tropospheric aerosol particles, J. Geophys. Res., 111, D23S32, doi:10.1029/2006JD007340, 2006.

Nash, K. L., Sully, K. J., and Horn, A. B.: Observations on the interpretation and analysis of sulfuric acid hydrate infrared spectra, J. Phys. Chem. A, 105, 9422–9426, 2001.

Qaddouri, A. and Lee, V.: The Canadian Global Environmental Multiscale model on the Yin-Yang grid system, Q. J. Roy. Meteor. Soc., 137, 1913–1926, doi:10.1002/qj.873, 2011.

Rice, A. L., Tyler, S. C., McCarthy, M. C., Boering, K. A., and Atlas, E.: Carbon and hydrogen isotopic compositions of stratospheric methane: 1. High-precision observations from the NASA ER-2 aircraft, J. Geophys. Res., 108, 4460, doi:10.1029/2002JD003042, 2003.

Richard, C., Gordon, I. E., Rothman, L. S., Abel, M., Frommhold, L., Gustafsson, M., Hartmann, J.-M., Hermans, C., Lafferty, W. J., Orton, G. S., Smith, K. M., and Tran, H.: New section of the HITRAN database: collision-induced absorption (CIA), J. Quant. Spectrosc. Ra., 113, 1276–1285, 2012.

Rinsland, C. P., Chiou, L. S., Boone, C., and Bernath, P.: Carbon dioxide retrievals from Atmospheric Chemistry Experiment solar occultation measurements, J. Geophys. Res., 115, D03105, doi:10.1029/2009JD012081, 2010.

Rothman, L. S., Gordon, I. E., Babikov, Y., Barbe, A., Benner, D. C., Bernath, P. F., Birk, M., Bizzocchi, L., Boudon, V., Brown, L. R., Campargue, A., Chance, K., Cohen, E. A., Coudert, L. H., Devi, V. M., Drouin, B. J., Fayt, A., Flaud, J. M., Gamache, R. R., Harrison, J. J., Hartmann, J. M., Hill, C., Hodges, J. T., Jacquemart, D., Jolly, A., Lamouroux, J., Le Roy, R. J., Li, G., Long, D. A., Lyulin, O. M., Mackie, C. J., Massie, S. T., Mikhailenko, S., Müller, H. S. P., Naumenko, O. V., Nikitin, A. V., Orphal, J., Perevalov, V., Perrin, A., Polovtseva, E. R., Richard, C., Smith, M. A. H., Starikova, E., Sung, K., Tashkun, S., Tennyson, J., Toon, G. C.,

AMTD
7, 1691–1747, 2014

Tyuterev, V. G., and Wagner, G.: The HITRAN 2012 molecular spectroscopic database, J. Quant. Spectr. Ra., 130, 4–50, 2013.

Schuck, T. J., Brenninkmeijer, C. A. M., Slemr, F., Xueref-Remy, I., and Zahn, A.: Greenhouse gas analysis of air samples collected onboard the CARIBIC passenger aircraft, Atmos. Meas. Tech., 2, 449–464, doi:10.5194/amt-2-449-2009, 2009.

Schwartz, M. J., Lambert, A., Manney, G. L., Read, W. G., Livesey, N. J., Froidevaux, L., Ao, C. O., Bernath, P. F., Boone, C. D., Cofield, R. E., Daffer, W. H., Drouin, B. J., Fetzer, E. J., Fuller, R. A., Jarnot, R. F., Jiang, J. H., Jiang, Y. B., Knosp, B. W., Krüger, K., Li, J.-L. F., Mlynczak, M. G., Pawson, S., Russell III, J. M., Santee, M. L., Snyder, W. V., Stek, P. C., Thurstans, R. P., Tompkins, A. M., Wagner, P. A., Walker, K. A., Waters, J. W., and Wu, D. L.: Validation of the Aura Microwave Limb Sounder temperature and geopotential height measurements, J. Geophys. Res., 113, D15S11, doi:10.1029/2007JD008783, 2008.

Sheese, P. E., Strong, K., Llewellyn, E. J., Gattinger, R. L., Russell III, J. M., Boone, C. D., Hervig, M. E., Sica, R. J., and Bandoro, J.: Assessment of the quality of OSIRIS mesospheric temperatures using satellite and ground-based measurements, Atmos. Meas. Tech., 5, 2993–3006, doi:10.5194/amt-5-2993-2012, 2012.

Sica, R. J., Izawa, M. R. M., Walker, K. A., Boone, C., Petelina, S. V., Argall, P. S., Bernath, P., Burns, G. B., Catoire, V., Collins, R. L., Daffer, W. H., De Clercq, C., Fan, Z. Y., Firanski, B. J., French, W. J. R., Gerard, P., Gerding, M., Granville, J., Innis, J. L., Keckhut, P., Kerzenmacher, T., Klekociuk, A. R., Kyrö, E., Lambert, J. C., Llewellyn, E. J., Manney, G. L., McDermid, I. S., Mizutani, K., Murayama, Y., Piccolo, C., Raspollini, P., Ridolfi, M., Robert, C., Steinbrecht, W., Strawbridge, K. B., Strong, K., Stübi, R., and Thurairajah, B.: Validation of the Atmospheric Chemistry Experiment (ACE) version 2.2 temperature using ground-based and space-borne measurements, Atmos. Chem. Phys., 8, 35–62, doi:10.5194/acp-8-35-2008, 2008.

Sioris, C. E., Boone, C. D., Bernath, P. F., Zou, J., McElroy, C. T., McLinden, C. A.: ACE observations of aerosol in the upper troposphere and lower stratosphere from the Kasatochi volcanic eruption, J. Geophys. Res., 115, D00L14, doi:10.1029/2009JD013469, 2010.

Stratospheric Processes and their Role in Climate (SPARC): SPARC Report No. 2: SPARC Assessment of Upper Tropospheric and Stratospheric Water Vapour, WCRP No. 113, WMO/TD-No. 1043, 312 pp., 2000.

AMTD
7, 1691–1747, 2014

Teffo, J.-L., Daumont, L., Claveau, C., Valentin, A., Tashkun, S. A., and Perevalov, V. I.: Infrared spectra of the $^{16}O^{12}C^{17}O$ and $^{16}O^{12}C^{18}O$ species of carbon dioxide: the region 500–1500 cm^{-1}, J. Mol. Spectrosc., 213, 145–152, 2002.

Toth, R. A., Line positions and strengths of CO_2 in the 1200–1430-cm^{-1} region, Appl. Optics, 24, 261–274, 1985.

Wiegel, A. A., Cole, A. S., Hoag, K. J., Atlas, E. L., Schauffler, S. M., and Boering, K. A.: Unexpected variations in the triple oxygen isotope composition of stratospheric carbon dioxide, P. Natl. Acad. Sci. USA, 110, 17680–17685, doi:10.1073/pnas.1213082110, 2013.

Wofsy, S. C., HIPPO science team, and cooperating modellers and satellite teams: HIAPER Pole-to-Pole Observations (HIPPO): fine-grained, global-scale measurements of climatically important atmospheric gases and aerosols, Philos. T. Roy. Soc. A, 369, 2073–2086, doi:10.1098/rsta.2010.0313, 2011.

AMTD
7, 1691–1747, 2014

Table 1. N_2 CIA microwindows: center frequencies, widths, and tangent height ranges in order of increasing lower TH limit.

Centre frequency (cm^{-1})	Microwindow width (cm^{-1})	Lower TH (km)	Upper TH (km)
2500.70	3.50	5	10
2505.50	3.00	5	15
2500.70	3.00	10	15
2492.10	2.00	10	18
2489.73	0.46	13	18
2485.10	0.60	13	20
2480.33	0.16	14	22
2473.02	0.23	15	22
2463.90	0.24	15	22
2462.00	1.60	15	23
2439.94	0.40	18	24
2430.21	0.80	21	25

AMTD
7, 1691–1747, 2014

Table 2. CO_2 microwindows: centre frequencies, widths, and tangent height ranges in order of increasing centre frequency.

Centre frequency (cm^{-1})	Width (cm^{-1})	Lower TH (km)	Upper TH (km)
1371.80	0.30	15	25
1372.52	0.30	20	25
1379.25	0.30	15	20
1380.70	0.35	15	25
1383.65	0.40	17	25
1384.42	0.45	15	25
1385.90	0.35	15	25
2604.50	0.80	5	25
2609.80	0.45	5	20
2610.56	0.20	5	20
2611.30	0.35	5	20
2612.04	0.20	5	25
2616.45	0.20	6	25
2617.18	0.20	7	20
2620.11	0.16	8	20
2620.83	0.18	5	20
2621.50	0.35	15	25
2623.75	0.30	15	20
2624.46	0.16	8	25
2625.18	0.16	8	20
2626.63	0.20	5	20
2627.35	0.20	5	25
2629.50	0.18	5	25
2629.50	0.20	8	25
2632.36	0.20	7	25
2633.79	0.20	8	25
2636.63	0.35	5	25

AMTD
7, 1691–1747, 2014

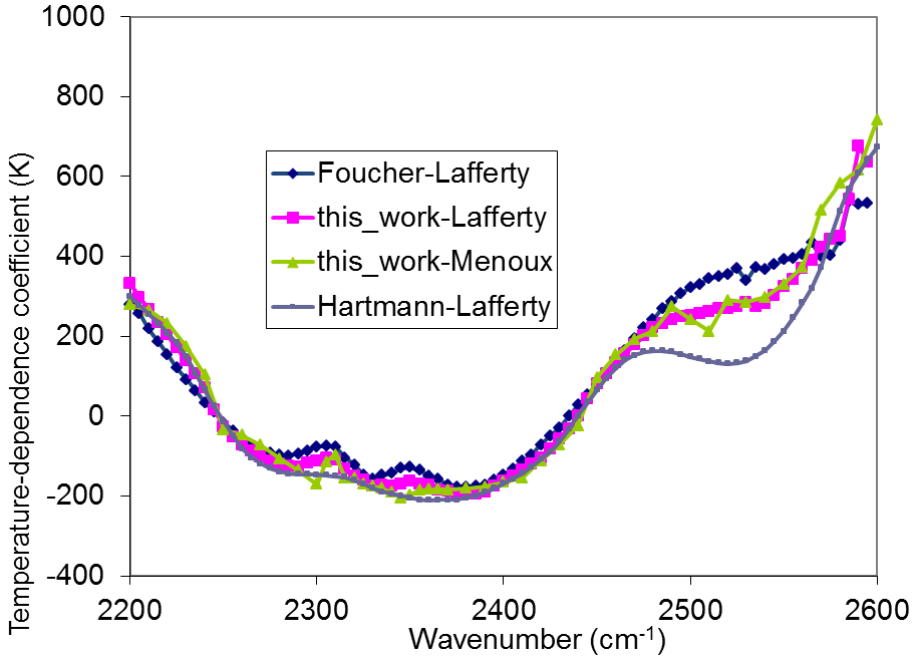

Fig. 1. Temperature dependence of N_2 CIA determined using the empirical model of Lafferty et al. (1996). The pink squares were determined in this work, while previous attempts were made by Hartmann (Lafferty et al., 1996) in blue-grey and Foucher (2009) in dark blue using the same dataset. Also shown in green is the temperature-dependence model parameter determined here using the less precise measurements of Menoux et al. (1993).

AMTD
7, 1691–1747, 2014

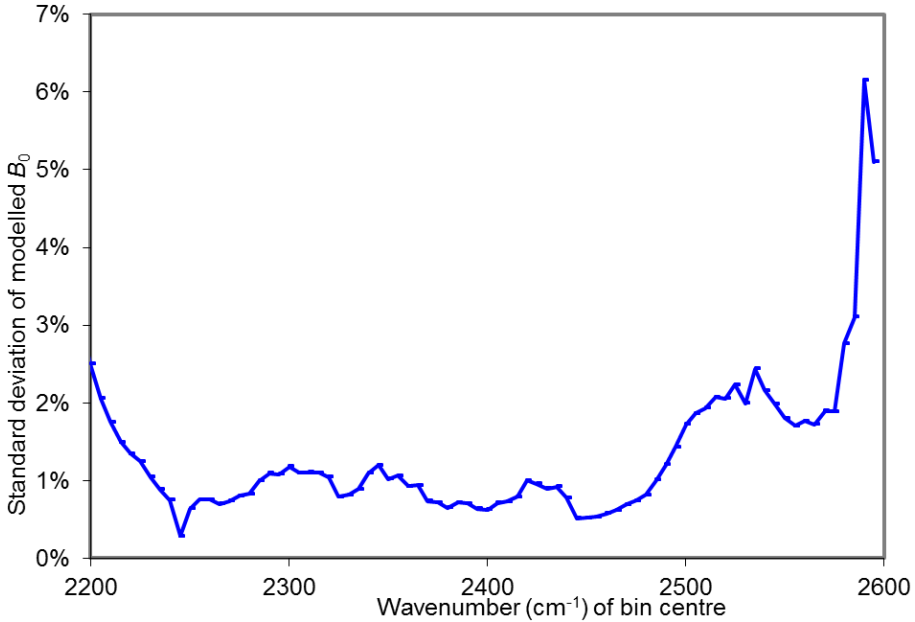

Fig. 2. Variability of five B_0 estimates (one from each temperature) calculated using the derived temperature dependence from Fig. 1 and by isolating B_0 in Eq. (1).

AMTD
7, 1691–1747, 2014

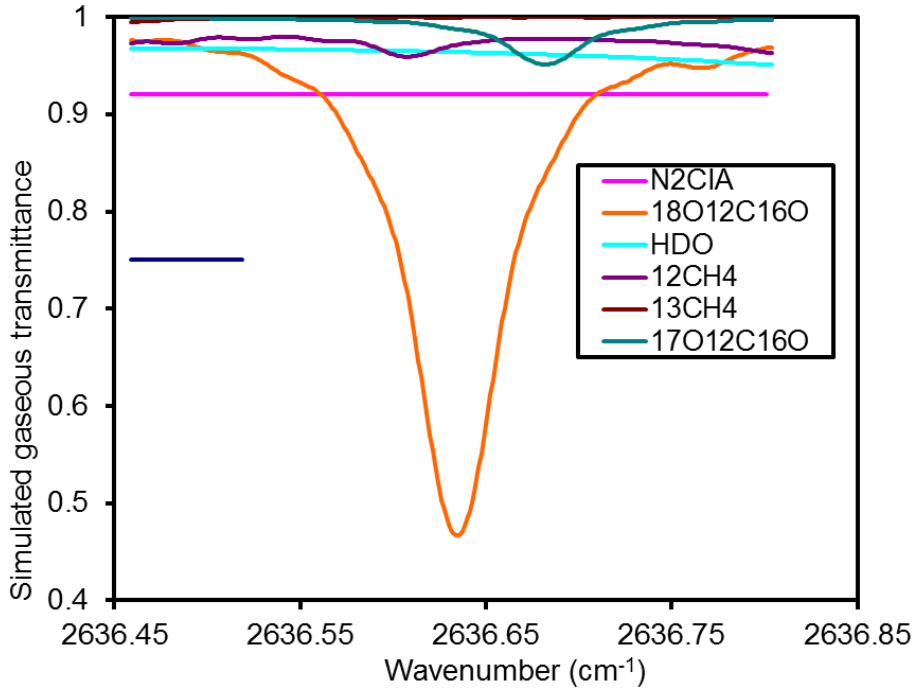

Fig. 3. Transmittance contributions from various gaseous absorbers in the 2637 cm^{-1} microwindow at TH = 6.3 km. Other gases may provide trivial contributions. The portion of the microwindow used to determine aerosol transmittance is shown in dark blue. The corresponding transmittance value of 0.75 is meaningless (only the wavenumber range is relevant).

AMTD
7, 1691–1747, 2014

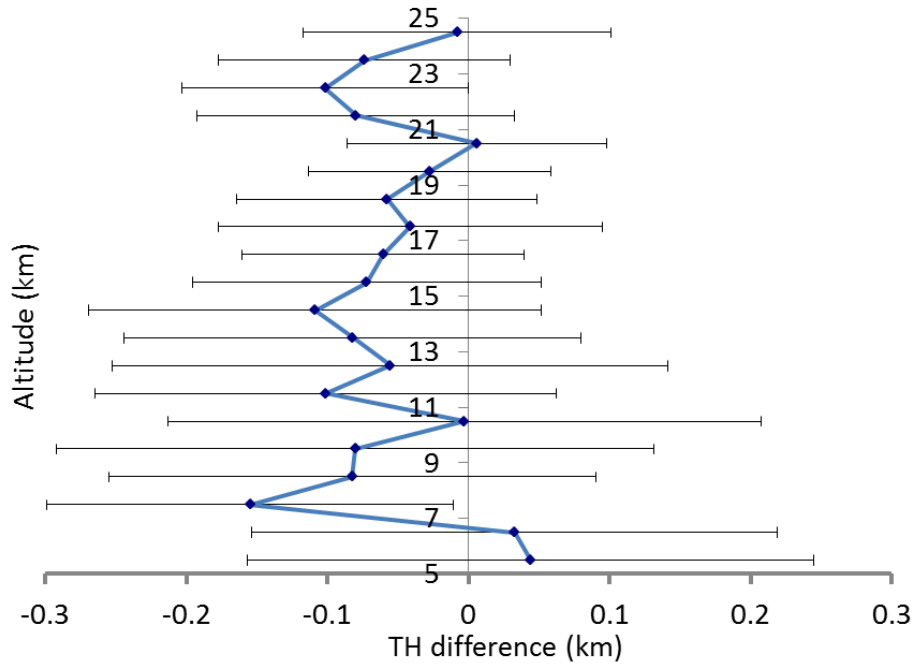

Fig. 4. TH differences (this work minus ACE v3.x) averaged over 120 randomly selected occultations covering latitudes in the range 80° N to 68° S and spanning from January 2009 to January 2011. The error bars indicate the standard deviation of these differences. Note that each occultation does not provide data at all altitudes because of the TH sampling is typically 2 km but varying with beta angle and the lowest tangent height is often determined by the altitude of high, optically thick cloud.

AMTD
7, 1691–1747, 2014

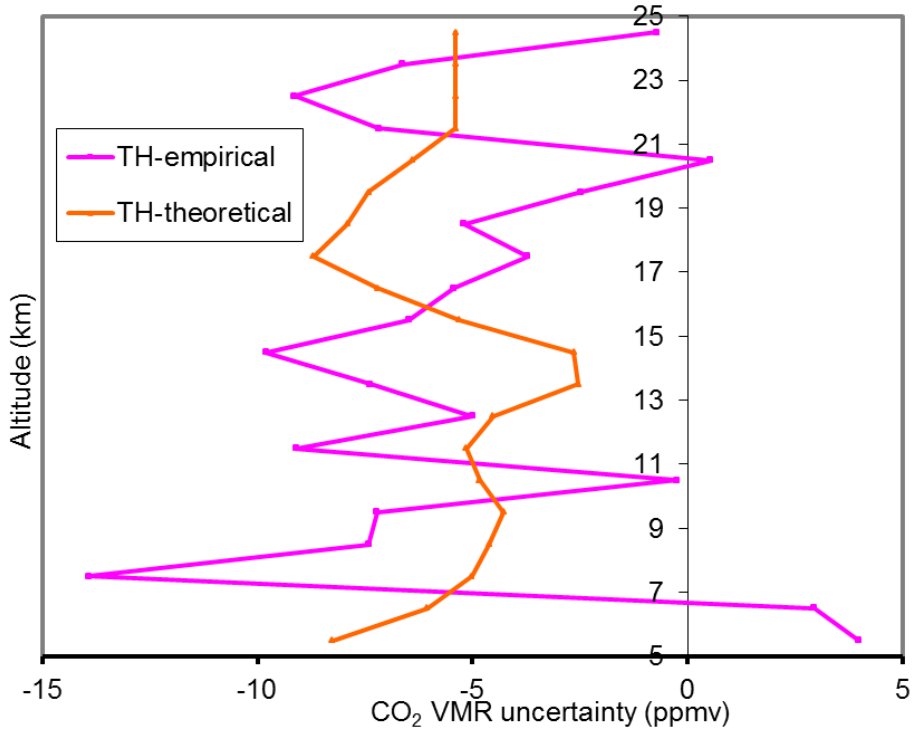

Fig. 5. CO_2 VMR uncertainty vs. altitude due to tangent height uncertainty from two different methods. "TH-empirical" propagates the observed TH differences vs. those retrieved using the ACE v3.x algorithm and "TH-theoretical" includes all of the individual sources of TH-related error added in quadrature.

AMTD
7, 1691–1747, 2014

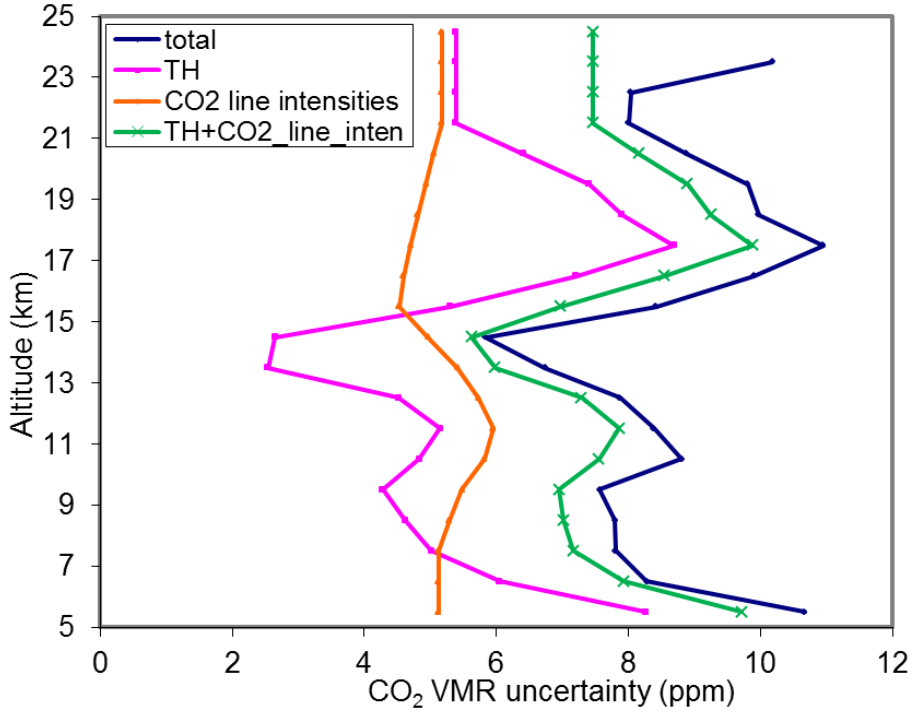

Fig. 6. Overall error budget for ACE including TH-related contributions.

AMTD
7, 1691–1747, 2014

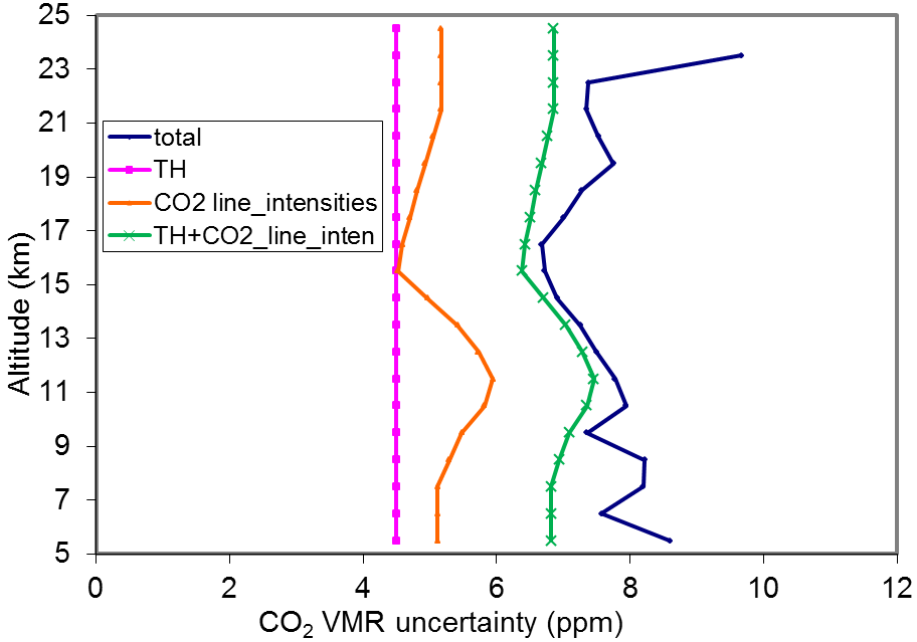

Fig. 7. Total CO_2 error budget for CASS-FTS, plus dominant individual terms. TH uncertainty is labelled "TH". The combination of TH and CO_2 line intensity uncertainties is labelled "TH+CO2_line_inten" and serves to demonstrate that these two sources of error account for the majority of the total error.

AMTD
7, 1691–1747, 2014

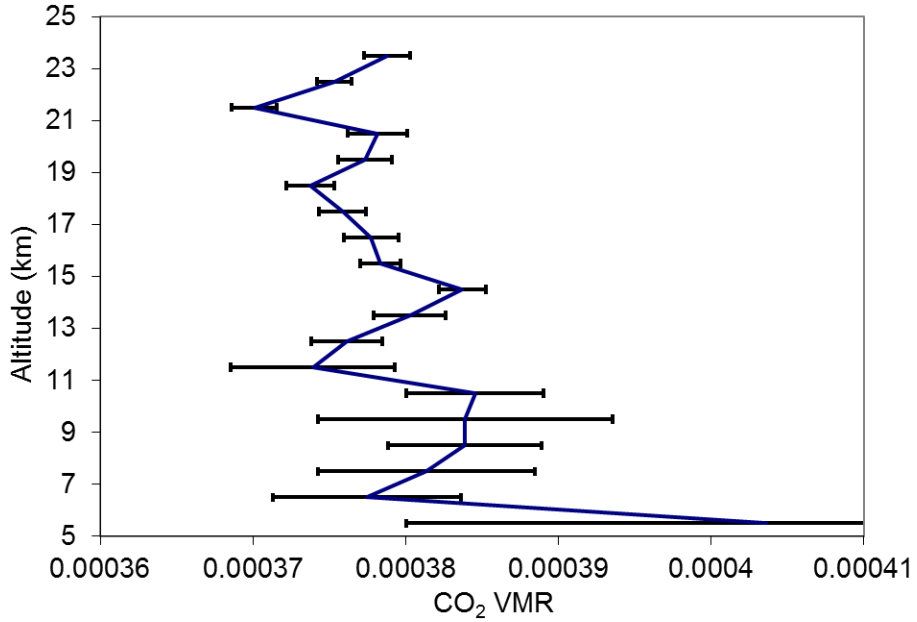

Fig. 8. Three-year (2009–2011) global median of cloud-free CO_2 VMR in the 5–25 km range (869 profiles). The error bar shows the standard error at each 1 km altitude bin (centered at 5.5 to 23.5 km).

AMTD
7, 1691–1747, 2014

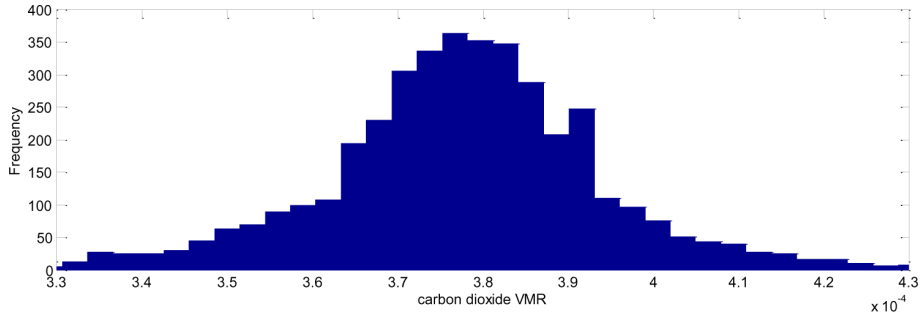

Fig. 9. Histogram of retrieved cloud-free CO_2 VMR at all altitudes (5–25 km), globally, in the 2009–2011 time frame. Outside of this range, the frequency distribution tends to be random (no resemblance to a Gaussian).

AMTD
7, 1691–1747, 2014

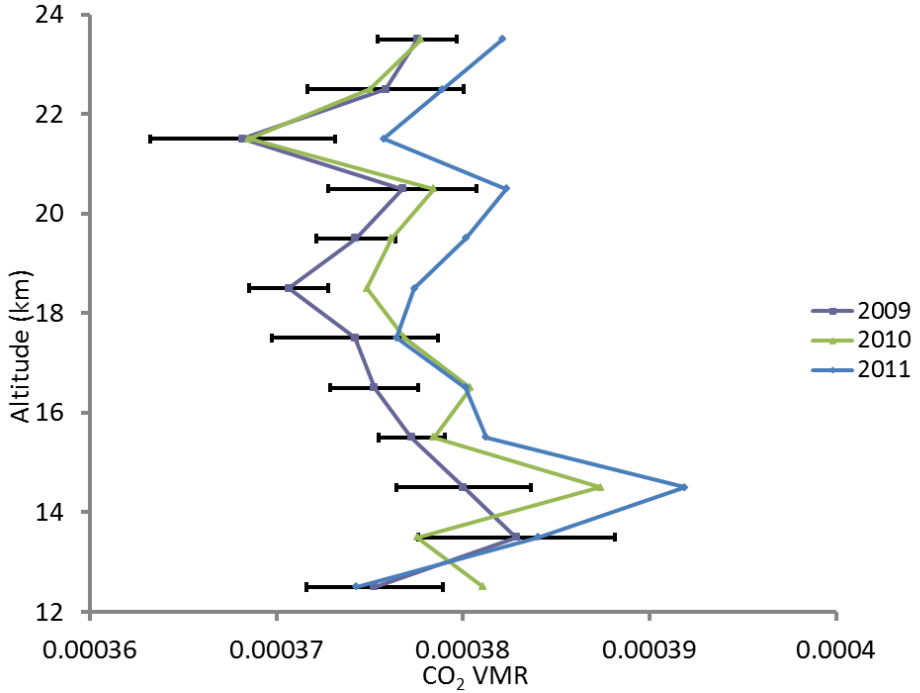

Fig. 10. Annual growth of CO_2 vs. altitude using yearly medians from the cloud-free dataset. Error bars show the standard error for 2009. Between 12 and 25 km and over all latitudes, the growth rate is 2.1 to 2.8 ppm yr^{-1}, or 2.5 ± 0.7 ppm yr^{-1} averaged over 2009–2011.

AMTD
7, 1691–1747, 2014

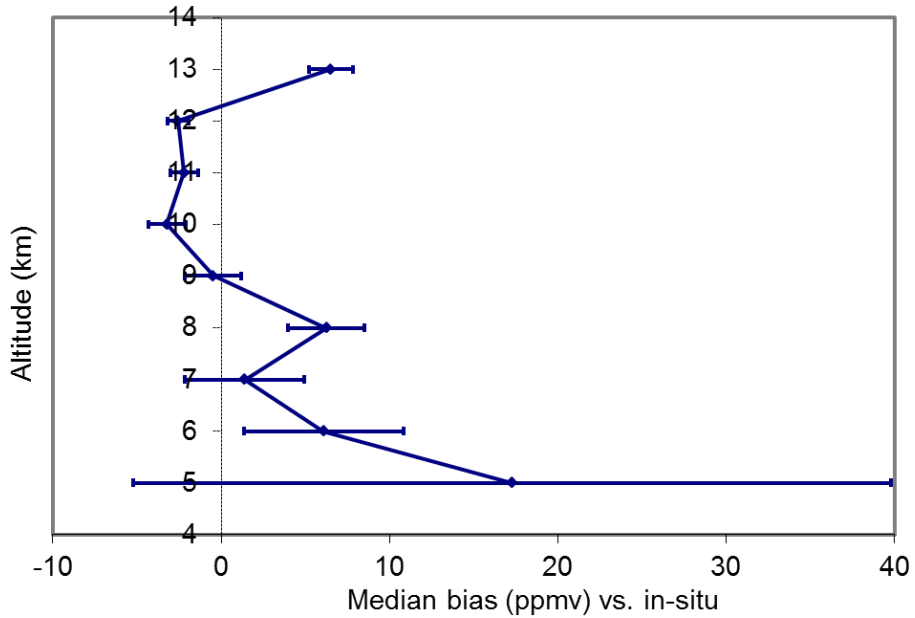

Fig. 11. Validation results by height, combining all latitudes. The error bar is the standard error of the bias. Sample sizes (N) are > 20 in the 7–13 km range.

AMTD
7, 1691–1747, 2014

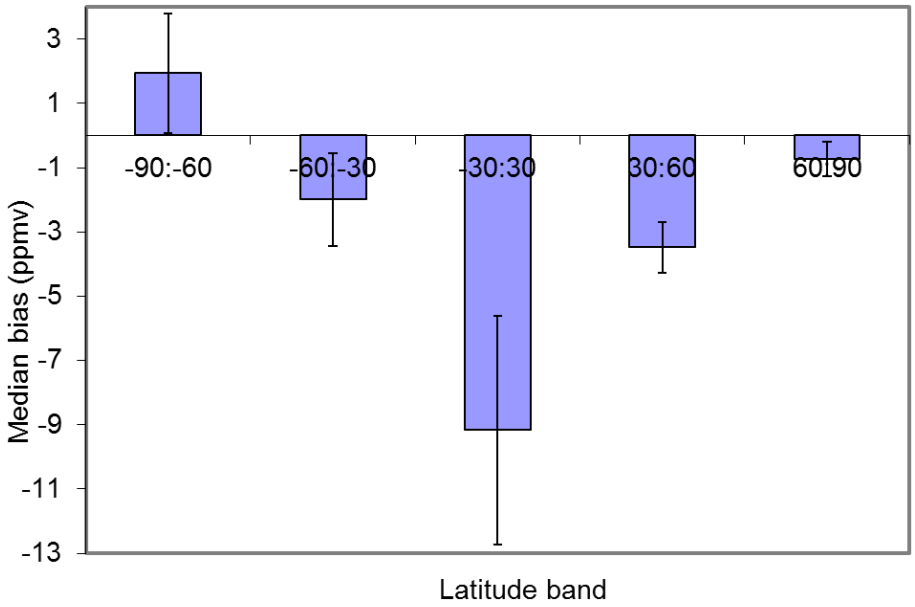

Fig. 12. Validation by latitude band combining all heights. The error bar is the standard error of the ensemble of pairwise biases.

AMTD
7, 1691–1747, 2014

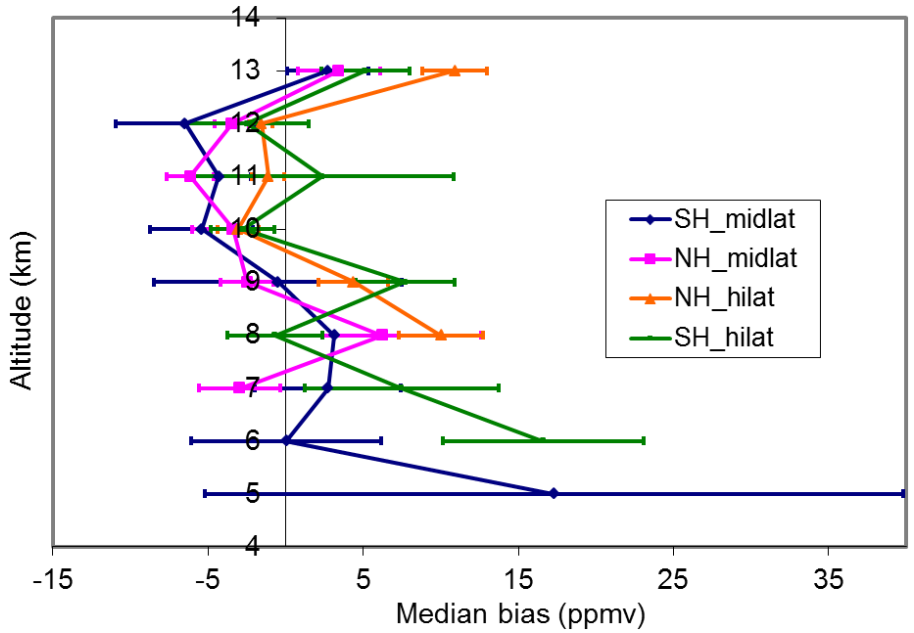

Fig. 13. Same as Fig. 11 but only for high and mid-latitude regions.

AMTD
7, 1691–1747, 2014

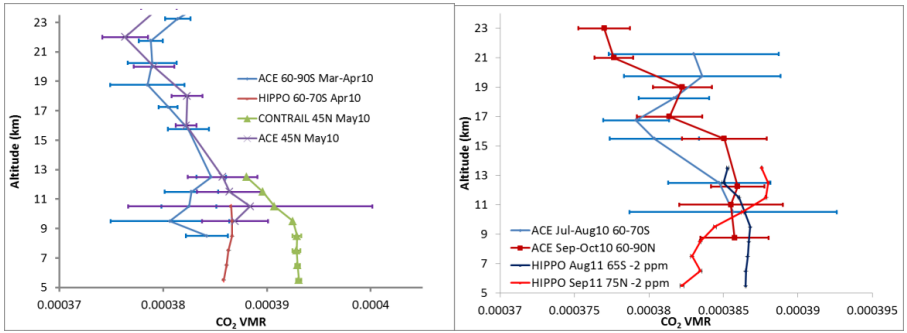

Fig. 14. (left) Latitudinal gradient in CO_2 VMR observed in boreal spring using satellite-based observations (ACE-FTS) and in in-situ data (HIPPO and CONTRAIL). All measurements are from the year 2010. The 45° N band comprises measurements from 30–60° N for both ACE-FTS and CONTRAIL. Medians are shown for ACE-FTS to reduce sensitivity to outliers while averages are shown for HIPPO and the error bars are the standard errors for both instruments. For CONTRAIL, we plot the average 3 sub-bands (30–40, 40–50, and 50–60° N) and each error bar represents the standard error of the 3 sub-band averages at that altitude. ACE-FTS data points between 13.0 and 15.0 km are excluded due to aerosol extinction (affects THs). 1.5 km and 2 km vertical bins are used above 15.0 km to improve sample sizes per bin, particularly above 19.0 km for the ACE-FTS profiles of March–April 45° N and May 60–70° N. (right) Same as left panel but for boreal summer. HIPPO measurements are from the year 2011, so we subtract 2 ppm to account for the annual growth.

AMTD
7, 1691–1747, 2014